Petroleum Science 21 (2024) 806–822

Contents lists available at ScienceDirect

Petroleum Science

journal homepage: www.keaipublishing.com/en/journals/petroleum-science

Original Paper

Depositional model of the Member Deng-2 marginal microbial mound-bank complex of the Dengying Formation in the southwestern Sichuan Basin, SW China: Implications for the Ediacaran microbial mound construction and hydrocarbon exploration

Jin-Min Song [a, *], Xin Jin [a], Zhong Luo [b], Shu-Gen Liu [a, c], Shao-Bo Liu [b], Xing-Zhi Ma [b], Zhi-Wu Li [a], Xue-Song Lu [b], Ling-Li Zhao [a], Ke-Ran Li [a], Jia-Xin Ren [a], Li-Zhou Tian [a], Hao-Shuang Deng [a]

[a] State Key Laboratory of Oil and Gas Reservoir Geology and Exploitation, Chengdu University of Technology, Chengdu, 610059, Sichuan, China
[b] PetroChina Research Institute of Petroleum Exploration and Development, Beijing, 100083, China
[c] Xihua University, Chengdu, 610039, Sichuan, China

ARTICLE INFO

Article history:
Received 13 November 2022
Received in revised form
16 June 2023
Accepted 5 December 2023
Available online 12 December 2023

Edited by Jie Hao and Teng Zhu

Keywords:
Sichuan Basin
The Member Deng-2
Marginal microbial mound-bank complex
Depositional model
Exploration implications

ABSTRACT

Recent advances in hydrocarbon exploration have been made in the Member Deng-2 marginal microbial mound-bank complex reservoirs of the Dengying Formation in the western Sichuan Basin, SW China, where the depositional process is regarded confusing. The microfacies, construction types, and depositional model of the Member Deng-2 marginal microbial mound-bank complex have been investigated using unmanned aerial vehicle photography, outcrop section investigation, thin section identification, and seismic reflections in the southwestern Sichuan Basin. The microbialite lithologic textures in this region include thrombolite, dendrolite, stromatolite, fenestral stromatolite, spongiostromata stone, oncolite, aggregated grainstone, and botryoidal grapestone. Based on the comprehensive analysis of "depositional fabrics–lithology–microfacies", an association between a fore mound, mound framework, and back mound subfacies has been proposed based on water depth, current direction, energy level and lithologic assemblages. The microfacies of the mound base, mound core, mound flank, mound cap, and mound flat could be recognized among the mound framework subfacies. Two construction types of marginal microbial mound-bank complex have been determined based on deposition location, mound scale, migration direction, and sedimentary facies association. Type Jinkouhe microbial mound constructions (TJMMCs) develop along the windward margin owing to their proximity to the seaward subfacies fore mound, with a northeastwardly migrated microbial mound on top of the mud mound, exhibiting the characteristics of large-sized mounds and small-sized banks in the surrounding area. Type E'bian microbial mound constructions (TEMMCs) primarily occur on the leeward margin, resulting from the presence of onshore back mound subfacies, with the smaller southwestward migrated microbial mounds existing on a thicker microbial flat. The platform margin microbial mound depositional model can be correlated with certain lateral comparison profile and seismic reflection structures in the 2D seismic section, which can provide references for future worldwide exploration. Microbial mounds with larger buildups and thicker vertical reservoirs are typically targeted on the windward margin, while small-sized microbial mounds and flats with better lateral connections are typically focused on the leeward margin.

1. Introduction

The upper Ediacaran Dengying Formation is the oldest and most ultradeep natural gas-producing strata in the Sichuan Basin. The

* Corresponding author.
E-mail address: songjinmin2012@cdut.edu.cn (J.-M. Song).

https://doi.org/10.1016/j.petsci.2023.12.005

hydrocarbon exploration activities began in the 1960s in the Leshan–Longnüsi paleouplift and its adjacent area. There were several breakthroughs during these explorations. The Weiyuan gasfield, discovered in 1964, was the oldest large-scale gasfield in China with 400 × 10^8 m^3 in proved geological reserves (Wei et al., 2008). In 1994, Ziyang gasfield was discovered with 102 × 10^8 m^3 in probable reserves (Liu et al., 2008; Chen et al., 2017; Sun et al., 2017). The borehole GS1 targeted on the Dengying Formation of central Sichuan Basin in 2011 achieved a daily production of up to 138.15 × 10^4 m^3 (Zou et al., 2014), with 3697 × 10^8 m^3 in proved geological reserves among the GS1 well area (Wei et al., 2015a; Luo et al., 2015; Yang et al., 2019). Recently, the borehole PT1 obtained a daily production reaching up to 121.98 × 10^4 m^3 in Member Deng-2 of the Dengying Formation, which indicates a considerable exploration prospect along the eastern margin of the Mianyang-Changning intracratonic sag in the western Sichuan Basin (Zhao et al., 2020; Xie et al., 2022). Furthermore, the probable geological reserves of the Dengying Formation in the Sichuan Basin have increased up to 1 × 10^{12} m^3(Zou et al., 2014; Luo et al., 2015; Wei et al., 2015a, 2015b; Song et al., 2017; Yang et al., 2019; Xie et al., 2022).

The reservoir rocks of the Dengying Formation in the upper Yangtze block were described as 'blue-green algae boundstone' (Zhang et al., 1996; Wei et al., 2008; Zou et al., 2014; Luo et al., 2015), which are reclassified as microbial (cyanobacteria) boundstone (Luo et al., 2013; Peng et al., 2014; Song et al., 2017, 2018; Lan et al., 2019; Xu et al., 2020; Luo et al., 2022). Further, the microbialite-dominated platform margin, intraplatform flat, and restrict lagoon have been recognized in depositional facies with large-scale marginal and patchy intraplatform microbial mound-bank complexes (Zou et al., 2014; Chen et al., 2017; Hu et al., 2019; Wang et al., 2021). The marginal mound-bank complex was primarily distributed along the passive cratonic and intracratonic sag margins (Zou et al., 2014; Luo et al., 2015; Yang et al., 2019, 2020), which comprised laminate, thrombolite, stromatolite, and spongiostromata dolostone (Chen et al., 2017; Song et al., 2017, 2018; Luo et al., 2022). Furthermore, the depositional architectures of the alternating marginal mound-bank complex and transgressive dolomudstone of Member Deng-4 have been identified in the central Sichuan Basin along the eastern rugged margin of the Mianyang-Changning intracratonic sag (Hu et al., 2019; Yang et al., 2020; Wang et al., 2021). The platform margin keep-up mound-bank, platform margin catch-up mound-bank, and intraplatform give-up mound-bank complexes of Member Deng-4 have been recognized in the microbial constructions of mound base, mound core, mound flank, mound cap, and mound flat in microfacies (Liu et al., 2013; Chen et al., 2017; Lan et al., 2019; Xu et al., 2020). In addition, recent research on depositional models of marginal microbial mound-bank complex has examined various factors, including paleogeomorphology, nutrient supply, ocean hydrodynamics, tides, winds, and atmospheric pressure (Tomas et al., 2013; Purkis et al., 2019; Zhang et al., 2021). The windward high tidal exchange grainstone zone and leeward whitings zone have been partitioned among the platform margin according to the current intensity and direction for the Great Bahama Bank (Purkis et al., 2019). However, the textures, depositional model, and evolution characteristics of the Member Deng-2 are totally underestimated. The Member Deng-2 windward and leeward microbial mound-bank complex constructions as well as a depositional model of the upper Ediacaran Dengying Formation in the E'bian-Jinkouhe area of the southwestern Sichuan Basin (Fig. 1(a)) were analyzed in this study using unmanned aerial vehicle photography, outcrop section measurement, thin section identification, and seismic reflections. The goal is to determine the significance of the Ediacaran microbial mound construction process and future worldwide hydrocarbon explorations.

2. Geological settings

The Ediacaran strata are the first sedimentary covering bed of the Yangtze craton, which is occupied by shallow-water carbonate platform constructions with a thickness of 650–1000 m in the upper Yangtze craton (Zou et al., 2014; Wei et al., 2015a, 2015b; Luo et al., 2015; Liu et al., 2016; Lan et al., 2019; Ding et al., 2021) (Fig. 1(a)–(c)). The coccoid cyanobacteria and filamentous cyanobacteria are dominant in the Ediacaran period, growing into microbial mats and mound-bank complexes in depositional constructions (Tomitani et al., 2006; Peng et al., 2014; Knoll, 2015; Liu et al., 2016; Song et al., 2017). According to microbe contents, textures, and lithologies, four members have been subdivided in the Dengying Formation, that is, the Member Deng-1, Deng-2, Deng-3, and Deng-4 in an upward direction (Deng et al., 2015; Wen et al., 2016) (Fig. 1(d)). The light-gray, thick-layered dolomudstone and laminated dolostone dominate the Member Deng-1 and are approximately 73–144 m thick. The Member Deng-2 is mostly occupied by light-gray thick-bedded to massive botryoidal and thrombolitic dolostones, with a thicknesses of 280–450 m, at the top of which is a regional unconformity separating the members Deng-2 and Deng-3. The bluish gray thin-bedded mudstone, argillaceous siltstone interbedded with dolomudstone, and tuff deposit in the Member Deng-3, which are 3–20 m thick owing to the Metazoan explosion of the *Gaojiashan* Fauna and *Shibantan* Fauna (Hua et al., 2007; Chen et al., 2008, 2014; Zhou et al., 2019). The gray to dark gray thick-bedded to massive laminate, stromatolite, and silica dolostone correspond to the Member Deng-4 with a thicknesses of 100–240 m (Liu et al., 2013; Zou et al., 2014; Luo et al., 2015; Liu et al., 2016; Song et al., 2017; Wen et al., 2016) (Fig. 1(d)). At the top of the Member Deng-4 a regional unconformity is developed, separating the Ediacaran from the Cambrian, which is overlain by dark carbonaceous thin-bedded mudstone, silica, and silty dolostone of the lower Cambrian Maidiping Formation (Zhao et al., 2022). The microbial mound primarily lies in the members Deng-2 and Deng-4 (Peng et al., 2014; Deng et al., 2015; Liu et al., 2016; Song et al., 2017; Xu et al., 2022). The outcrop sections are located along the southwestern margin of the upper Yangtze craton, including the villages Limingcun (LMC) and Zhentouba (ZTB) in Jinkouhe District of Leshan city and the Village Xianfeng (XF) in E'bian county (Fig. 1(b) and (c)).

The Mianyang-Changning intracratonic sag has been discovered in the western Sichuan Basin, lasting from the late Ediacaran to the early Cambrian (Liu et al., 2013, 2017; Du et al., 2014; Zou et al., 2014). However, its extension's starting time is still disputed. Some scholars argue that the sag was generated earlier in the Nanhua period and continued to expand during the Ediacaran period in which the members Deng-3 and Deng-4 were deposited in deep-water environments (Zou et al., 2014; Wei et al., 2015a, 2015b; Zhou et al., 2015; Jiang et al., 2016; Wen et al., 2016; Chen et al., 2017; Lan et al., 2019). Other scholars argue that no such tectonic extensions occurred during the early Ediacaran period that yield depositional facies lagoon, restricted platform, intraplatform basin, or deep-water shelf in the Yangtze craton (Liu et al., 2015; Zhou et al., 2015; Xing et al., 2015). From the late Ediacaran to early Cambrian, the upper Yangtze craton could not begin to extend and thus resulted in sag formation (Liu et al., 2013). Current research demonstrates that the typical botryoidal textures have been identified by cutting thin sections of the boreholes GS17 and ZY1, allowing a central sag to be identified (Chen et al., 2017; Li et al., 2018), which are distinctive depositional-diagenetic products of the Member Deng-2 on the shallow-water platform (Qian et al., 2017; Ding et al., 2019; Zhai et al., 2020). Therefore, this study

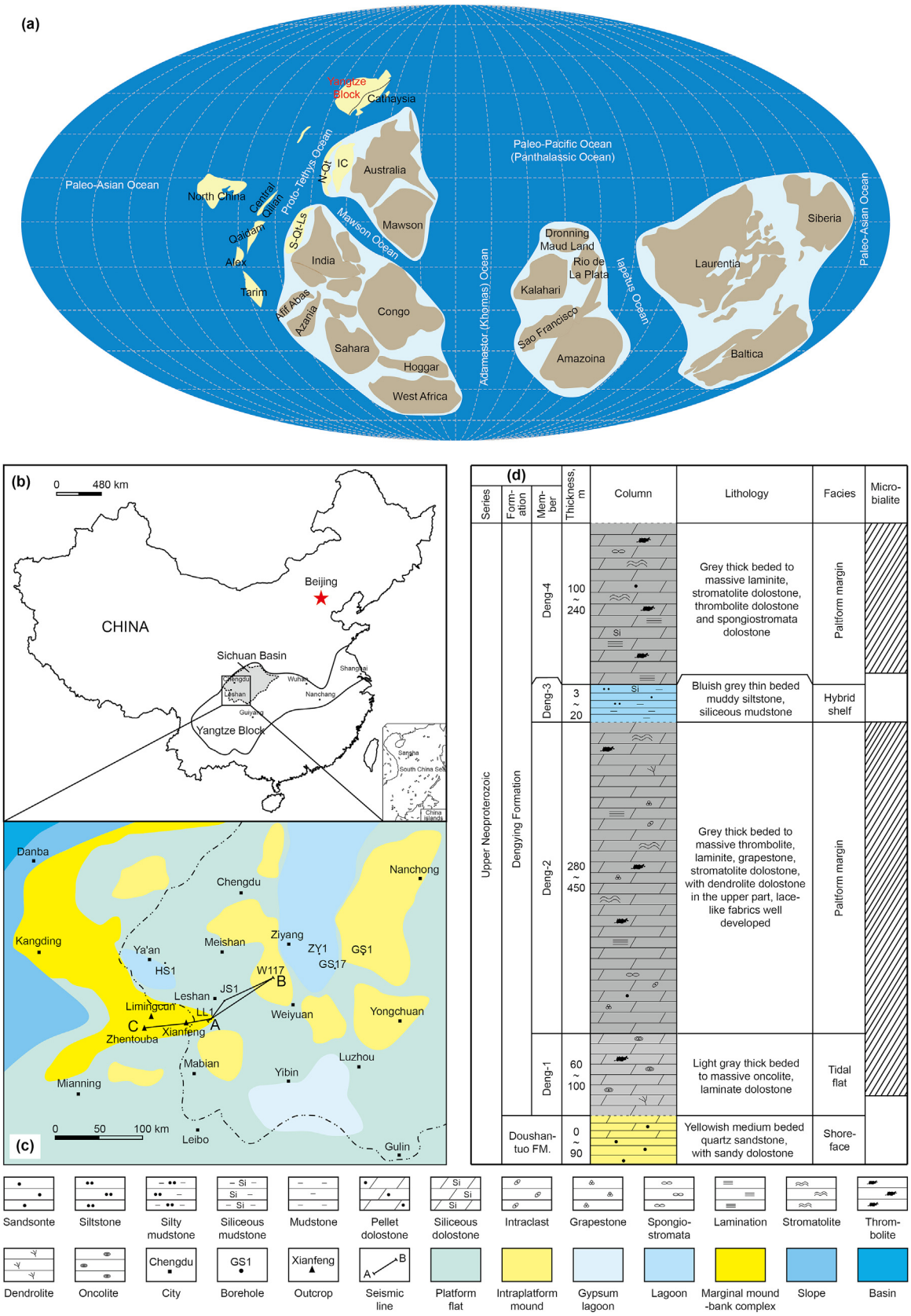

Fig. 1. Paleoplate reconstruction map **(a)**, the location **(b)**, depositional facies **(c)**, and strata column **(d)** of the Member Deng-2 in the Dengying Formation, southwestern Sichuan Basin (modified after Liu et al., 2015; Song et al., 2017, 2018; Zhao et al., 2018).

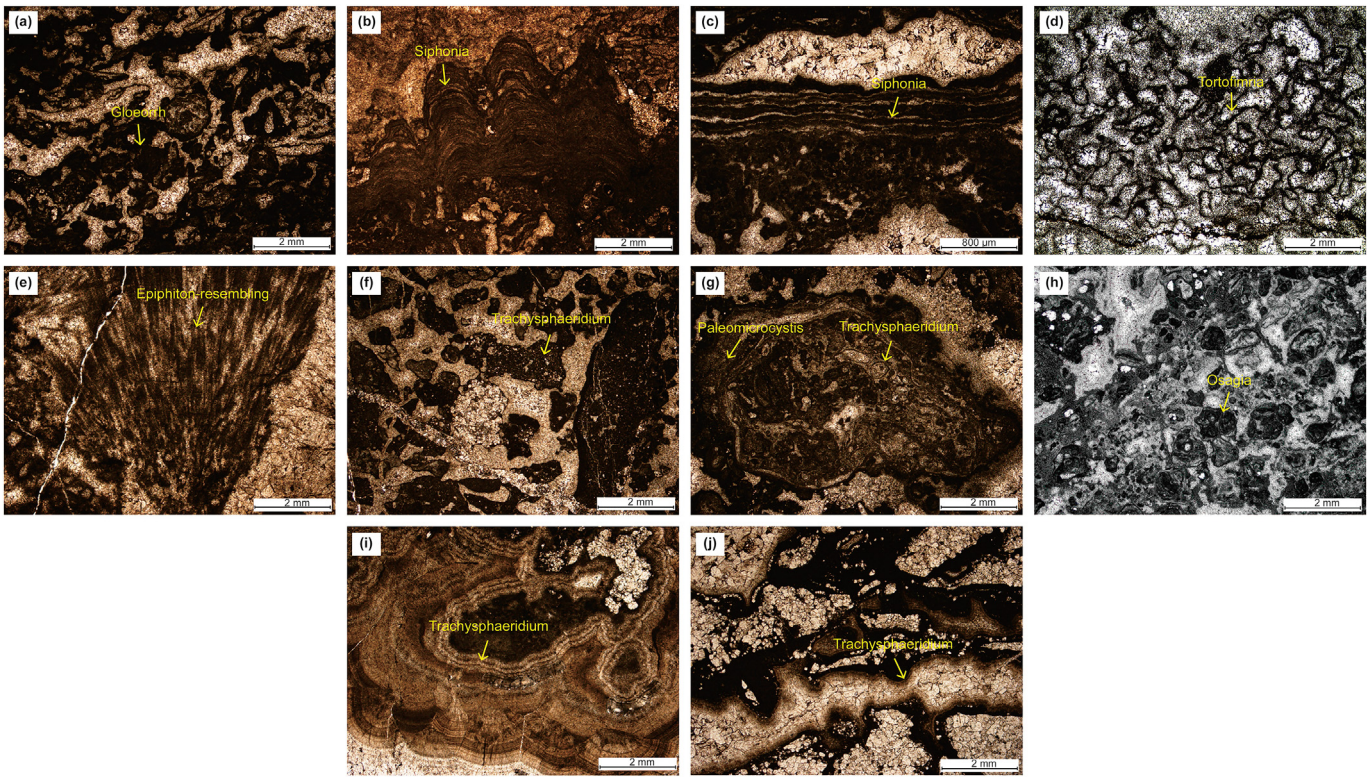

Fig. 2. Microbe assemblages, microbial fabrics, and lithologic textures of the Member Deng-2 in the Dengying Formation, southwestern Sichuan Basin
Abbreviation captions for MA: MA1- *Gloeorrh alveus* Tsao et Zhao and *Balios*; MA2- *Actinophycus divaricatus* Yin (sp. Nov.), *Phacelofimbria emeishanensis* Tsao et Zhao, *Acus Muricatus* Tsao et Zhao, and *Epiphiton-resembling*; MA3- *Girvanella-resembling* sp., *Praesolenopora*, and *Siphonia* sp.; MA4-*Renaclis-resembling* and *Tortofimria dictyotos* Tsao et Zhao; MA5-*Trachysphaeridium* sp., *Osagia* f., and *Paleomicrocystis*.
(a) Thrombolitic fabric related to *Gloeorrh alveus* Tsao et Zhao (MA1) form thrombolite (LT1), EB22-6, outcrop section Zhentouba; **(b)** the stromatolitic fabric built by *Sophonia* (MA3) lead to stromatolite (LT3), EB12-2, outcrop section Zhentouba; **(c)** the stromatolitic fabric associated with *Sophonia* (MA3) builds fenestral stromatolite (LT4), EB22-8, outcrop section Zhentouba; **(d)** spongiostromata fabric with *in situ Tortofimria dictyotos* Tsao et Zhao (MA4), forming spongiostromata stone (LT5), 5239.5 m, borehole HS1; **(e)** dendrolitic fabric with the brush-like *Epiphyton-resembling* (MA2) leads to dendrolite (LT2), EB15-2, outcrop section Zhentouba; **(f)** coated fabric resulting from *Trachysphaeridium* sp. (MA5) forms aggregated grainstone (LT7), EB21-8, outcrop section Zhentouba. **(g)** coated fabric by the *Paleomicrocystis* and *Trachysphaeridium* sp. (MA5) points to oncolite (LT6), EB17-8, outcrop section Zhentouba. **(h)** coated fabric related to *Osagia* f. (MA5) forming oncolite (LT6), XF31-2, outcrop section Xianfeng; **(i)** the coated fabric due to the *Trachysphaeridium* sp. (MA5) result in botryoidal grapestone (LT8), JKHII2-1, outcrop section Limingcun; **(j)** thrombolitic fabrics are coated by the laminated botryoidal fabrics related to *Trachysphaeridium* sp. (MA5) linking LT1 together with LT8, JKHII4–47, outcrop section Limingcun. All photographs were taken under plain polarized light.

adopts the second viewpoint, according to which the sag stretched interior upper Yangtze craton in later than the Chron Deng-3. Notably, slightly-rimmed carbonate platform, slope, and basin facies coexist in the Chron Deng-2 among the upper Yangtze, with a platform margin microbial mound-bank complex along Fengjie-Wanyuan-Ningqiang-Beichuan-E'bian-Kangding, as well as platform flat, mound, gypsum and restricted lagoons developing intraplatform (Liu et al., 2015; Zhou et al., 2015) (Fig. 1(b)).

3. Materials and methods

We carried out detailed field investigations, descriptions, and sampling of the outcrop sections in the Village Limingcun section, Zhentouba section, and Village Xianfeng section, collecting 362 pieces of samples in total. The microbial mound macrostructures were photographed using a series of phantom-4 advanced unmanned aerial vehicles from the China Dajiang company. Thin sections, stained with Alizarin Red-S and potassium ferricyanide (Dickson, 1965), were examined under a polarized microscope (Nikon Eclipse E600 POL). The microbe form identification was compared to the photo plates from the E'mei area in the southwestern Sichuan Basin published by Yin et al. (1980) and Song et al. (2018). Dunham's carbonate classification, which was put forth in 1962, has served as the basis for the lithologic research. The depositional facies and microfacies analyses were led by the idealized sequence of standard facies (Wilson, 1975). The platform margin division scheme was illustrated by the facies model of patch reefs and associated facies on a shelf (Longman, 1981; Tucker, 1985). The microfacies subdivision is performed based on the composite analysis of 'depositional fabrics–lithology–microfacies', revised from the idealized sequence of standard depositional facies and microfacies terminology (Wilson, 1975; Tucker, 1985; Feng, 2019). Scanning Electron Microscope-Energy Dispersive Spectrometer (SEM-EDS) analysis was performed using FESEM (Quanta 250 FEG, USA) and an energy spectrometer (Oxford INCAx-max20, UK) using a field emission lamp. Porosity and permeability measurements were performed on an automated permeameter–porosimeter (AP-608, USA). All analyses were performed at the State Key Laboratory of Oil and Gas Reservoir Geology and Exploitation at Chengdu University of Technology.

4. Results

4.1. Microbial fabrics and lithology in mound-bank complex of the Member Deng-2

The microbial fabrics of the Member Deng-2 in the southwestern Sichuan Basin comprises thrombolitic, stromatolitic,

Table 1
Description and interpretation of the microbe assemblages (MA) and lithologic textures (LT) in the microbial mound-bank complex of the Member Deng-2 (modified after Yin et al., 1980; Song et al., 2018).

LT	MA		Characteristics Description	Interpretation
LT1 Thrombolite	MA1	*Gloeorrh alveus* Tsao et Zhao	Irregular, dispersed, closely packed micrite clots in morphology, with dolosparite in coelom, fibrous dolomite lining cavity	Moderate- to high-energy environment of platform margin or intraplatform flat
		Balios pinguensis Tsao, Chen et Chu	Dense spotty morphology, consisting of irregular, unbranching, non-tapering micritic thread-like fabric with micritic body walls and dolospar cavity	
LT2 Dendrolites	MA2	*Actinophycus divaricatus* Yin (sp. Nov.)	Branching, short, radiated micritic thread-like fabric rooting from clot fabrics	High-energy environment of the platform margin
		Phacelofimbria emeishanensis Tsao et Zhao	In fasciculate growth, radiated hollow tubules with micritic body walls	
		Acus Muricatus Tsao et Zhao	Occur like short micritic thorns in morphology, densely-radiated perpendicular to the lamination	
		Epiphiton-resembling	Dark, clotted, branching texture, with dolospar cemented framework pores	
LT3 Stromatolites	MA3	*Girvanella-resembling* sp.	Unbranching, non-tapering micritic tubules with micritic body walls forming horizontal lamination	Moderate-energy environment of the platform margin or intraplatform flat
LT4 Fenestral stromatolites		*Praesolenopora fascicularis* Cao et Zhao	Tube-like in shape, with micritic body walls and dolosparite-filled intraskeletal voids	
		Siphonia sp.	In cone shape, with micritic body walls and dolosparite cemented voids	
LT5 Spongiostromata stone	MA4	*Renaclis-resembling*	Chamber structure and porous framework with fibrous isopachous dolomite lining the colonies	Moderate-energy environment of the platform margin or intraplatform flat
		Tortofimria dictyotos Tsao et Zhao	Bubble-like in morphology, micritic body walls, and dolosparite hollow cavity, with rounded, oval or even polygonal chambered structures	
LT6 Oncolite	MA5	*Trachysphaeridium* sp.	Condensed globular cluster, micritic body walls, and dolosparite hollow cavity lined by isopachous fibrous rims	Moderate- to high -energy environment of platform margin or interior platform
LT7 Grainstone		*Osagia* f.	Irregularly concentric lamination, 2–3 mm in diameter	
LT8 Grapestone		*Paleomicrocystis*	Circular or globular, dolomicrite inside, and dolosparite cemented coelom cavity	

spongiostromata, dendrolitic, and coated fabrics, as well as thrombolite, stromatolite, spongiostromata stone, dendrolite, oncolite, grapestone, and aggregated grainstone in lithology (Song et al., 2017, 2018), which belong to 'boundstone' in Dunham's carbonate rock classification published in 1962.

Thrombolites are dark, irregular, micritic clusters within light dolosparite in the mesoscope with a size of (1–3) mm × (1–4) mm, exhibiting isolated and coated forms under a microscope (Fig. 2(a)). Stromatolites are moundy, undulated, or stratified in the mesoscope that are 50–80 cm thick. They comprise interbedded, light-colored, silt-grained crystalline dolomite and dark microbial laminations in millimeters' thickness with the development of fenestral structure (Fig. 2(b) and (c)). Spongiostromata stone is a light-gray, thick-layered to massive fenestral dolostone observed in the mesoscope and characterized by an irregular, foam-like framework in the microscope (Fig. 2(d)). Dendrolites are also observed in the Zhentouba outcrop section, with shrub clusters and light-colored dolosparite in the mesoscope. Arborescent clusters are dark micritic bifurcated thalli growing upward and outward in the length of 4–6 mm (Fig. 2(e)). Aggregated grainstone predominantly comprises micritized doloarenite and dolorudite (lumps), which are associated with peloids and some coated grains in lobate outline (Flügel, 2010). Most grains have thin rims of light-gray fibrous early-marine cement, with clean, drusy dolomite cement lining the remaining interparticle pores (Fig. 2(f)). Oncolites are related to the coated fabrics with light and dark laminations encircling the dark irregular clot core with a thickness of 40–80 cm, as seen in the mesoscope. They occur in irregular, subround, or elliptical shape with clot core sizes of (1.0–2.0) mm × (0.5–3.0) mm and the encircling coated lamination with a thickness of 0.2–0.3 mm under the microscope (Fig. 2(g) and (h)). Grapestone, which comprises irregular clot core and botryoidal lamination (Fig. 2(i)), has microscopic dark and light lace-like lining structures including sedimentary stratiform lamination, karst lining lamination, and biofilm spherical lamination in millimeters' thickness (Song et al., 2018; Zhai et al., 2020). Further, grapestone, which is unique in the Member Deng-2, with granular dolomite cement occluding intraclot pores (Fig. 2(j)).

Different lithologic types are related to some certain microbe assemblages (MA) and lithologic textures (LT) related to thirteen microbe forms and one oncolite form (Yin et al., 1980; Song et al., 2018). The thrombolites (LT1) are associated with the irregular spotty or patchy microbe community of *Gloeorrh alveus* Tsao et Zhao and *Balios pinguensis* Tsao, Chen et Chu (MA1) (Fig. 2(a), Table 1). The dendrolites (LT2) results from the branching microbial community of *Actinophycus divaricatus* Yin (sp. Nov.), *Phacelofimbria emeishanensis* Tsao et Zhao, *Acus Muricatus* Tsao et Zhao and *Epiphiton-resembling* (MA2) (Fig. 2(e), Table 1). However, the stromatolites (LT3) or fenestral stromatolites (LT4) dominated by the tube-like community of *Girvanella-resembling* sp., *Praesolenopora fascicularis* Cao et Zhao and *Siphonia* sp. (MA3) (Fig. 2(b) and (c), Table 1). The spongiostromata stone (LT5) is comprised by a bubble-like community of *Renaclis-resembling* and *Tortofimria dictyotos* Tsao et Zhao (MA4) (Fig. 2(d), Table 1). The oncolite (LT6), aggregated grainstone (LT7) and botryoidal grapestone (LT8) are relevant to the coated community of *Trachysphaeridium* sp., *Osagia* f. and *Paleomicrocystis* (MA5) (Fig. 2(f)–(i), Table 1) (Yin et al., 1980; Song et al., 2018). Moreover, the thrombolitic fabrics, which typically occur together with grapestones, are characterized by the laminated botryoidal lining fabrics (Fig. 2(j), Table 1).

4.2. Vertical depositional microfacies sequence of the microbial mound-bank complex of the Member Deng-2

Marginal mound-bank complexes show a fore mound, mound framework, and back mound subfacies association according to water depth, energy level, and lithologic assemblages. The microfacies of the mound base, mound core, mound flank, mound cap, and mound flat could be identified among the mound framework subfacies. Moreover, the microfacies of the mound flat and back mound lagoons dominate in the back mound subfacies, while the fore mound slope microfacies is prominent in the fore mound subfacies.

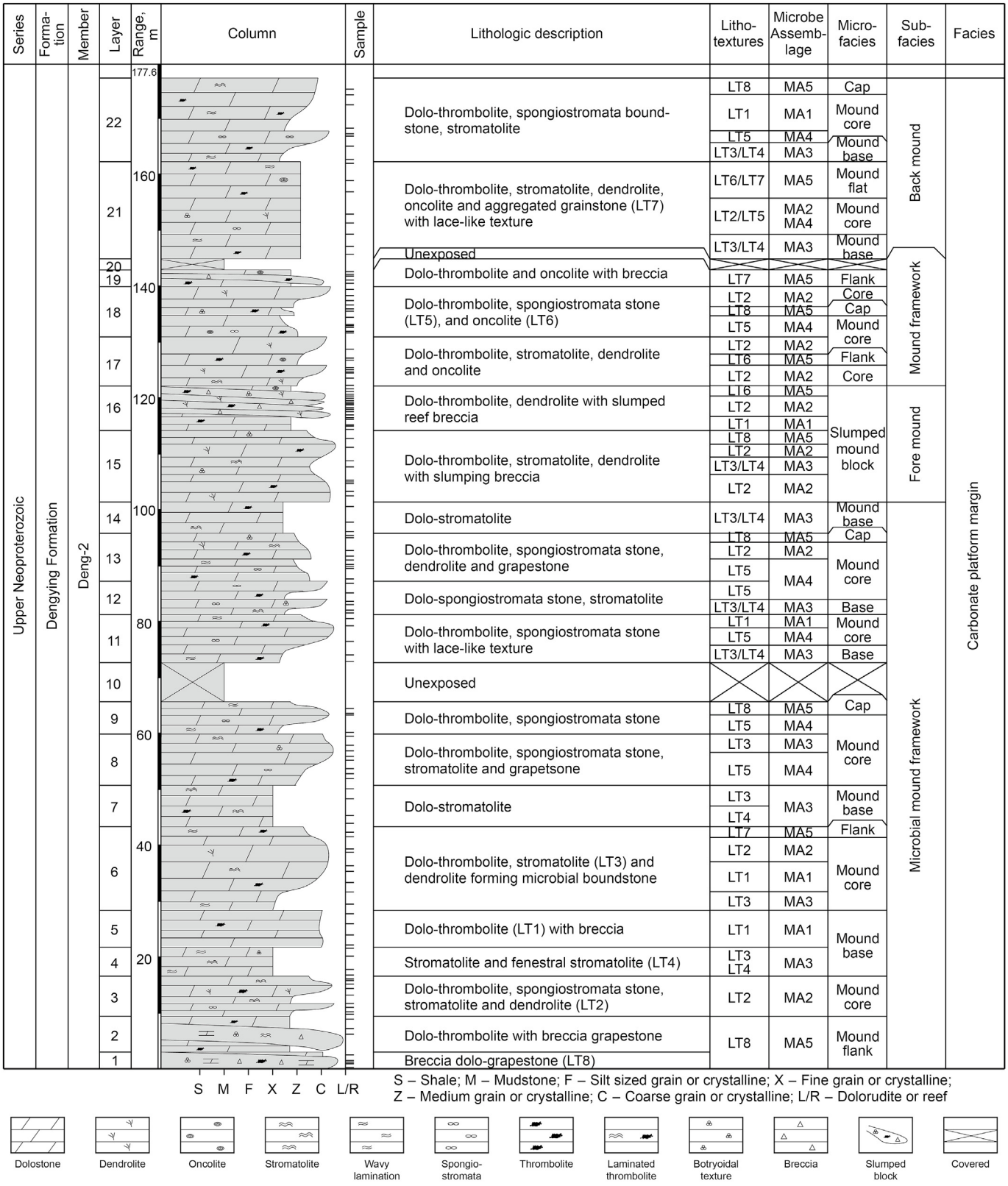

Fig. 3. Comprehensive microfacies evolution column of the Member Deng-2 in the Dengying Formation of outcrop section Zhentouba, southwestern Sichuan Basin.

Based on the 177.6 m outcrop section investigation and 147 pieces of thin section identification, the vertical depositional microfacies sequence was analyzed in the outcrop section Zhentouba. The mound framework, fore mound, and back mound develop in order from bottom to top in subfacies. Furthermore, nine mound construction cycles have been identified in microfacies

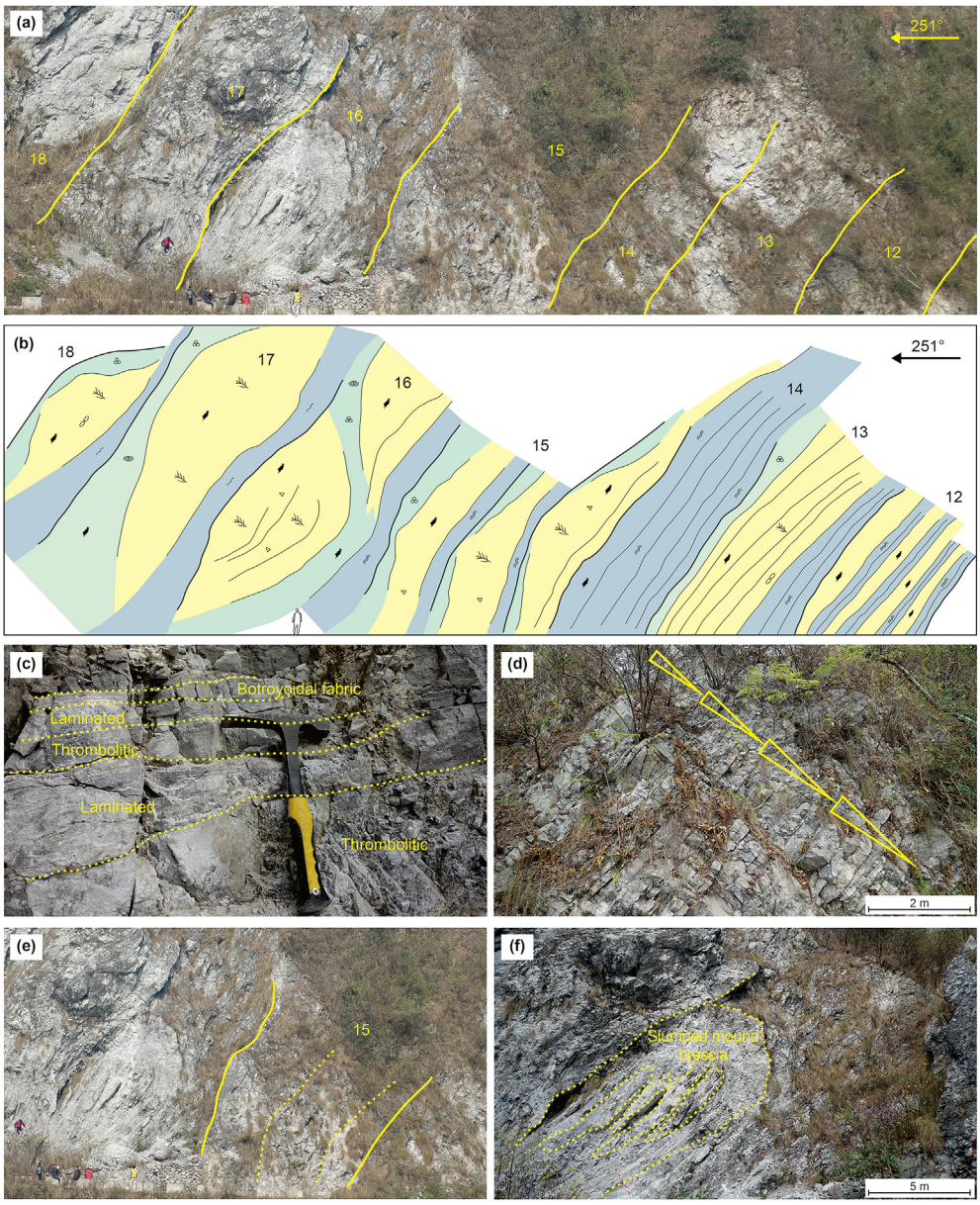

Fig. 4. Macroscopic structures of the Member Deng-2 mound-bank complex in Dengying Formation of outcrop section Zhentouba, southwestern Sichuan Basin
(a) Macroscope construction characteristics from the layers 12 to 18; **(b)** mound construction structure diagram of the layers 12 to 18; **(c)** decimeters' cycle of the layer 13, from thrombolitc, laminated layer to botryoidal fabrics (yellow dash lines); **(d)** merters' cycle of the layer 12, with four coarsening upward cycles (yellow triangles); **(e)** microbial mound constructions of the layer 15 in macroscope, with three stages of microbial mound aggradations (yellow dash lines); **(f)** four stages of slumped mound blocks in the upper part of layer 16, with slumping-dragging structure along the margin. The legends of **b** are the same as in Fig. 5.

vertically. The first cycle comprises mound flank and mound core in microfacies with a thickness of 18 m. Moreover, the microfacies of the mound base, mound core, and mound flank dominate the second cycle with a thickness of 20 m. The mound base, mound core, and mound cap microfacies associations occur in the third and fourth cycle with a thicknesses of 22–24 m. The microfacies of the mound core and mound flank dominate in the fifth to seventh cycle in thicknesses of 5–7 m. The microfacies associations of mound base, mound core, and mound flat or mound cap occur in the last two cycles with a thicknesses of 20–25 m (Fig. 3). Moreover, the slumping mound block microfacies developed in the fore mound subfacies.

In pace with the microfacies evolution from the mound base, mound core, mound flank to the mound cap, the microbe assemblages change from MA3, MA2, MA4, and MA1 to MA5 (Fig. 3). The microbial mound-bank complexes overlay each other vertically, inside which the microfacies of the mound base, mound core, and mound cap could be identified. Layers 12 to 16 of the Zhentouba section are representative in the microfacies sequence, with a total thickness of 41.8 m (Fig. 4(a)). Four meter-scale mound growth cycles develop in layer 12 in the macroscope (Fig. 4(b) and (d)). The lithologic textures change from fenestral stromatolites (LT4) and stromatolites (LT3) to thrombolites (LT1), with the microfacies evolving from the mound base to the mound core (Fig. 4(b)). The dark gray middle-layered thrombolite dolostone, laminated dolomudstone, and botryoidal grapestone (LT8) develop gradually upward within a single dm-scale cycle in the lithology in layer 13 (Fig. 4(c)) and form mound core and mound cap in

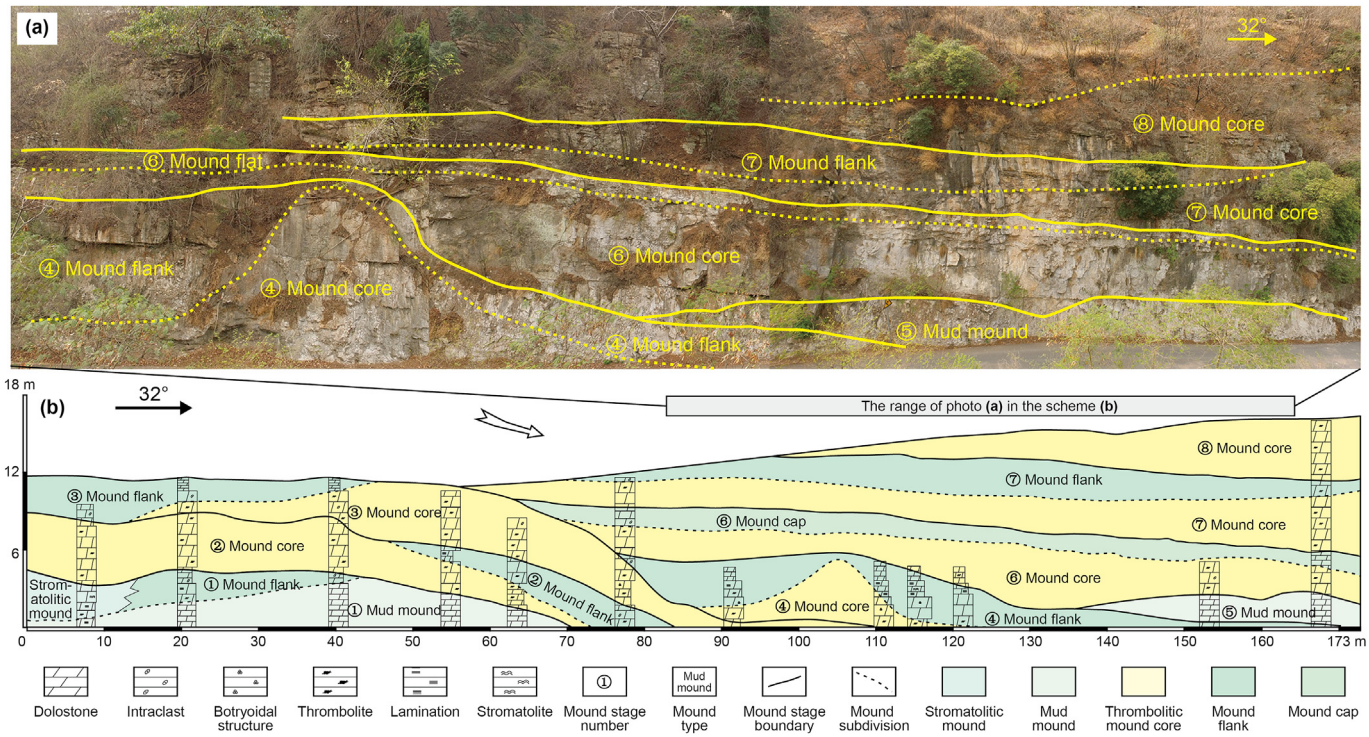

Fig. 5. Macroscope structure of the type Jinkouhe microbial mound constructions (TJMMCs) of the Member Deng-2 in the Dengying Formation based on unmanned aerial vehicle photography in the outcrop section of Village Limingcun, southwestern Sichuan Basin.

microfacies (Fig. 4(b) and (c)). However, the mound base microfacies dominated in layer 14, with LT3 and LT4 coming up (Fig. 4(b)). Further, the lithological textures change from dendrolites (LT2) and LT3 to LT8 gradually within layer 15, with breccia well developing, indicating three thick-bedded to massive slumping mound blocks overlaying vertically in the macroscope (Fig. 4(b) and (e)). Moreover, the thin-bedded, dolopackstone with graded bedding dominated in the lower part of layer 16, with a thickness of 8 m. The slumping mound blocks constitute the upper part with a size of 1.5 m × 6 m, 1.2 m × 10 m, 1.0 m × 6 m and 1.5 m × 12 m, respectively (Fig. 4(b) and (f)), which points to the fore mound subfacies.

4.3. Construction types of the microbial mound-bank complex of the Member Deng-2

The microbial mound-bank complexes of the Member Deng-2 primarily grow along the platform margin (Zou et al., 2014; Song et al., 2017; Zhang, 2017). Two types of platform margin microbial mound constructions have been found out in the southwestern Sichuan Basin, that is, Type Jinkouhe microbial mound constructions (TJMMCs) and Type E'bian microbial mound constructions (TEMMCs), based on the composite characteristics of their deposition location, current direction, mound scale, migration direction, and adjacent sedimentary facies association.

4.3.1. Characteristics of Type Jinkouhe microbial mound constructions

The TJMMCs have been investigated using unmanned aerial vehicle photography and multisite outcrop section measurements of the Village Limingcun. Three types of microbial mounds among TJMMCs can develop such as microbial mound, mud mound, and stromatolitic mound. The single microbial mound is 4–5 m thick in the central part, thinning to 2–3 m in both flanks and 70–80 m wide (Fig. 5(a)). The mud mound is 2–3 m in height and extends up to 30–70 m horizontally (Fig. 5(a)). The stromatolitic mound is of 3–4 m high and 10–15 m across. All the microbial mound constructions gradually migrate to the northeast (Fig. 5(b)).

Eight stages of mound constructions, including six stages of microbial mounds and two stages of mud mounds, typically occur in TJMMCs (Fig. 5(b)), with the mound core, mound flank, and mound cap being subdivided into microfacies. The first stage of construction comprises a mud mound with light gray, massive dolomudstone in the lithology (Fig. 6(a)). A mud mound flank that comprises pellet dolostone is located on the southwestern side of the mud mound core, turning into a stromatolitic mound horizontally instead, which is composed of light-dark laminations under both the mesoscope and microscope, with millimeters' relief. The thrombolitic mound lying on the stromatolitic mound constitutes the second stage of mound construction (Fig. 6(a)). The irregular clots bounding together lead to framestone under a microscope, cemented by the fibrous dolomite (Fig. 6(c)). The wedge-shaped mound flank microfacies develops on the northeastern side of the mound core microfacies (Fig. 6(b)). The third stage of construction also includes a thrombolitic mound that is 10–20 m away from the second-stage mound to the northeast and is 4–5 m thick and 90–100 m across. The mound flank microfacies consists of dolograinstone and overlaps the northeastern side of the mound core (Figs. 5(b) and 6(d)). The thrombolitic mound dominates the fourth stage of the mound and is large, measuring 5–6 m high and 30–40 m across (Fig. 5(a)). However, the fifth stage of mound turns into a mud mound with light gray, massive construction in macroscope and pellet dolostone under a microscope (Fig. 6(e)). The spongiostromata mounds occur in the sixth stage of mound construction, above which is the mound cap microfacies dominated by laminated dolomudstone (Fig. 6(f)). The last two stages of the microbial mounds overlap each other in the macroscope, with the mound flank microfacies of the seventh stage of the mound along

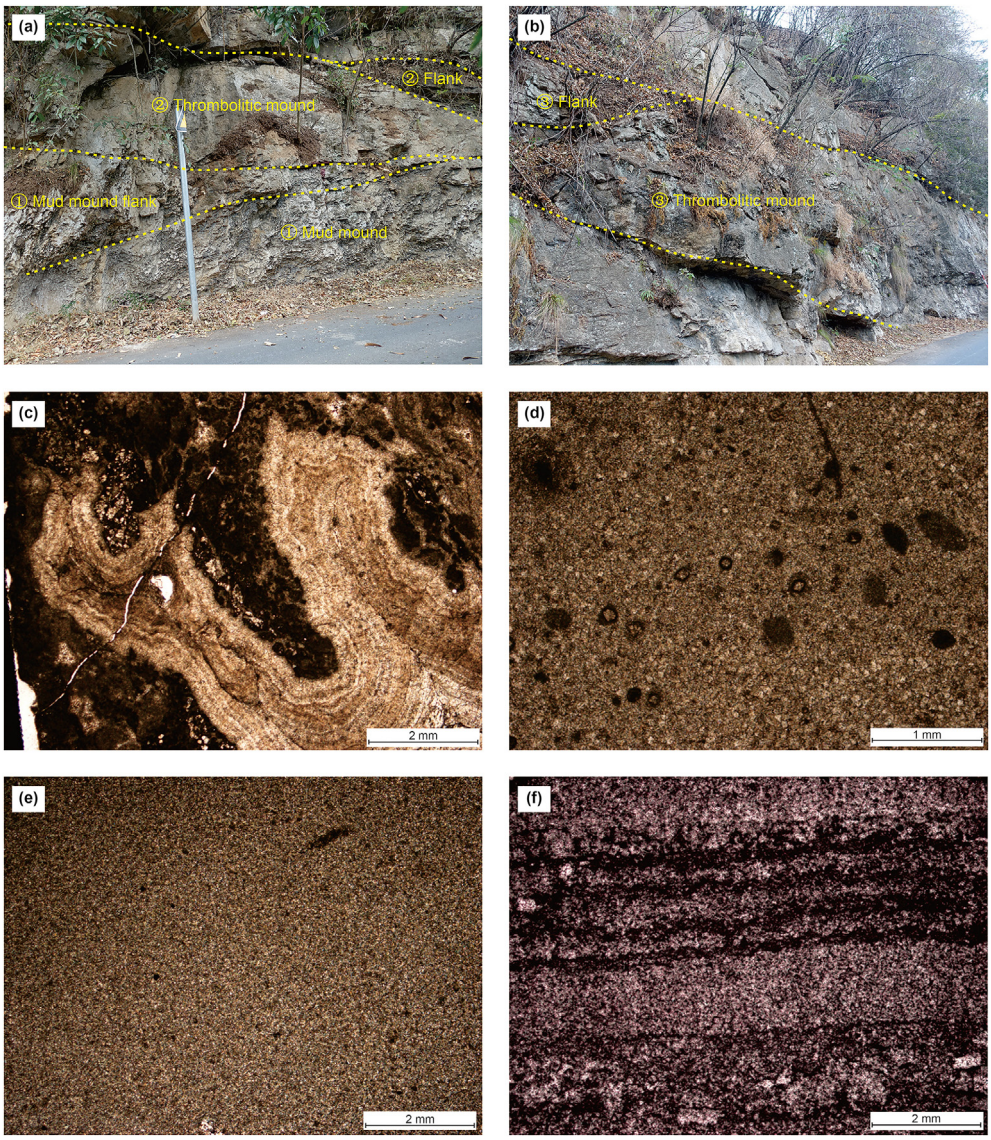

Fig. 6. Mesoscope and microscope structures of the Member Deng-2 TJMMCs in the Dengying Formation, southwestern Sichuan Basin
(a) the first stage of mud mound and the second stage of thrombolitic mound in layer 1 to 2 in mesoscope with mound core and mound flank in microfacies; **(b)** characteristics of mound core and mound flank among the third stage of thrombolitic mound in the layer 3 in mesoscope; **(c)** thrombolitic fabric of the second stage of microbial mound under microscope, with the irregular clot bounding together to form framework, JKHII2-3, plane polarized light; **(d)** grainstone in mound flank of the third stage of thrombolitic mound, JKHII3-5, plane polarized light; **(e)** pellet dolostone among the fifth stage of mud mound under microscope, JKHII4-4, plane polarized light; **(f)** laminated fabric in the mound cap of the sixth mound under a microscope, JKHII5-16, plane polarized light.

the southwestern side (Fig. 5(a) and (b)).

The TJMMCs are adjacent to the fore mound slope horizontally, which is the extension seaward-facing part of the platform edge, with turbidites, slumped mound blocks, and *in situ* microbial mounds co-existing. Considering layers 16 and 17 in the outcrop section Zhentouba as examples, the thin layered turbidite dolo-packstone was located in the lower part of layer 16, with a centimeters-thick graded bedding in the mesoscope (Fig. 7(a)) and rounded microbial binding debris under a microscope (Fig. 7(d)). The slumped mound block develops in the upper part of the layer 16, with a breccia size of 10–20 cm to 1 m. The angular thrombolite dolostone breccia, 2.5–3 mm in size, dominated the slumped mound block with fibrous dolosparite (Fig. 7(e)). The *in situ* dendritic microbial mound of layer 17 lies above the slumped breccia, measuring 10 m × 22 m and thinning to both flanks (Fig. 4(a)). The broom-like or shrub-like cyanobacteria *in situ* grow into waving zonation in the mesoscope (Fig. 7(c)). Furthermore, *Actinophycus divaricatus* Yin (sp. Nov.) and *Epiphiton-resembling* (MA2) have been identified in the growth zonation based on the microbe fossil plate comparison (Yin et al., 1980; Song et al., 2018). The *Actinophycus divaricatus* Yin (sp. Nov.) lies in the inner growth zonation, while the *Epiphiton-resembling* grows in the outer zonation (Fig. 7(f)). The turbidites, slumped mound breccia, and *in situ* arborization microbial mounds have evolved gradually upward, indicating the falling process of sea level from the subfacies of the fore mound to the microbial mound framework.

4.3.2. Characteristics of the type E'bian microbial mound constructions

The TEMMCs have been investigated in the outcrop section of the Village Xianfeng. The TEMMCs are well exposed in layers 28–31 in the outcrop section, which are mostly thick-bedded to massive in

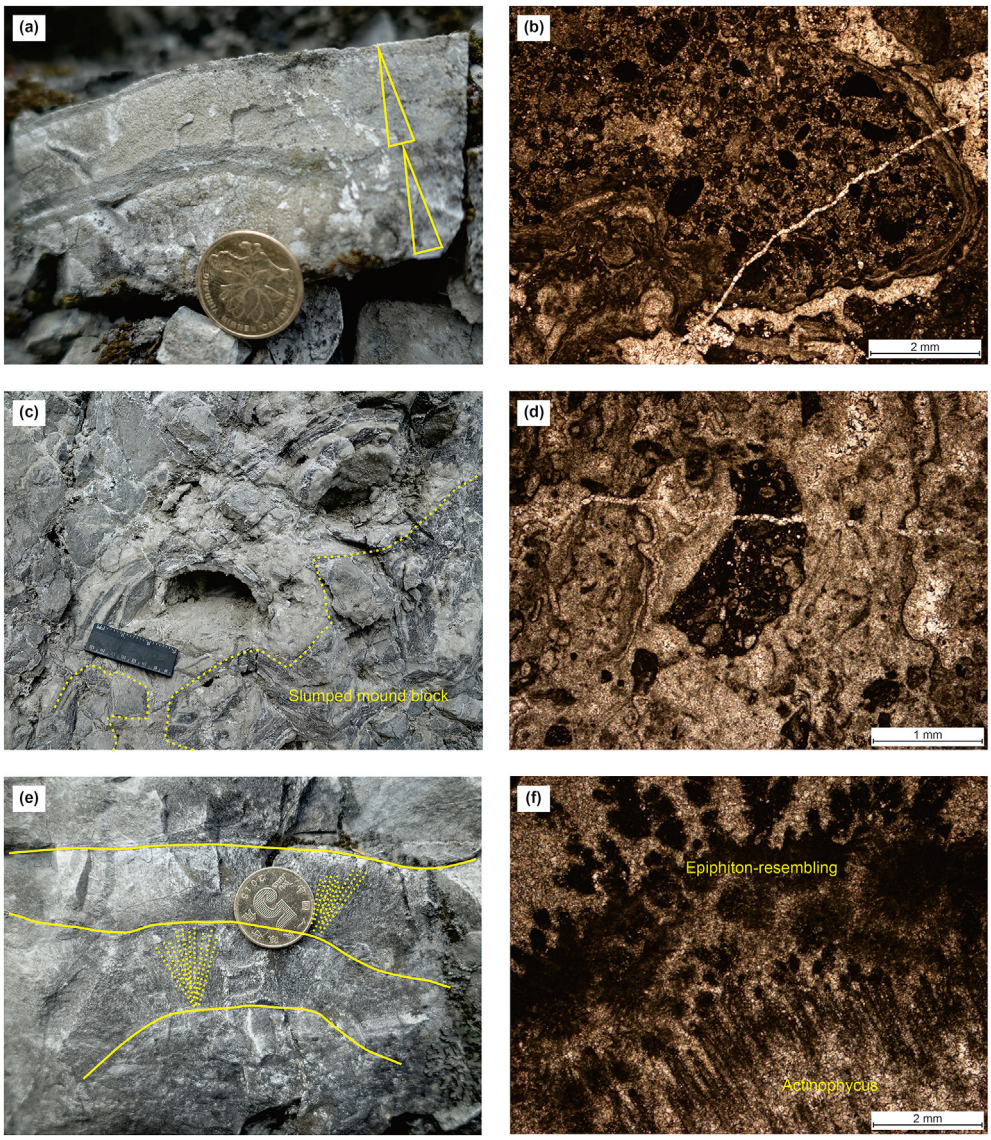

Fig. 7. Fore mound slope deposition characteristics of the Member Deng-2 in Dengying Formation of outcrop section Zhentouba, southwestern Sichuan Basin
(a) Turbidite with graded bedding in centimeter scale, in the lower part of layer 16; **(b)** rounded grains in the turbidite under microscope, with coarsening upward and coated by microbe lamination outside, EB16-12, plane polarized light; **(c)** mesoscopic characteristics of slumped mound blocks, with the botryoidal fabric coated the dark mound breccia in size of 10 cm–20 cm, in the upper part of layer 16; **(d)** thrombolite breccia under microscope, in size of 2.5 mm–3 mm, cemented by the dolosparite, EB16-15, plane polarized light; **(e)** broom or shrub-like microbe form irregular growing zonation in layer 17; **(f)** radial or shrub-like thalli of the *Actinophycus divaricatus* Yin (sp. Nov.) and *Epiphiton-resembling* under microscope in layer 17, with the *Epiphiton-resembling* growing above the *Actinophycus divaricatus* Yin (sp. Nov.), bifurcated thalli at an angle of 5–10°, EB17-9, plane polarized light.

the macroscope. Four stages of microbial mounds can be observed with a thickness of 2–3 m, thinning up to 1–2 m on both flanks and 40–50 m in length (Fig. 8(a)). The laminated or stromatolitic fabrics lead to a microbial flat in the macroscope, with wavy laminations in a total thickness of 4–5 m (Fig. 8(b)), which lies below the microbial mound constructions. The massive mound core and wedge-shaped mound flank could be observed in the outcrop section (Fig. 8(d)). The bounded clot fabrics consist of a mound core, among which is cemented by the laminated lining of fibrous dolomite (Fig. 8(c)). However, the mound flank is primarily occupied by stromatolitic dolostone with well-developed fenestral pores (Fig. 8(e)). The TEMMCs extend much farther horizontally, consisting of much more stromatolitic, microbial flat microfacies in the lower part and migrating southwestward (Fig. 8(b)).

The TEMMCs are terminated by the back mound lagoon horizontally in the onshore direction, which is behind the marginal microbial mound barriers. The thin-bedded light-gray and dark-gray couplets, 20–40 cm thick, develop in the outcrop section of the Village Xianfeng, with a total thickness of 36.2 m (Fig. 8(f)). The dark-gray layers are dominated by dolomudstone with wavy bedding, which is inferred to form in a relatively quiet environment. However, the light-gray layers comprise interbedded laminations of the microbial binding dolograinstone or dolopackstone in millimeters' scale under a microscope. The microbial binding grainstone laminations have a graded bedding with radially arranged grains (Fig. 8(g)) and a bottom scouring surface, indicating the effect of periodic storm currents. Furthermore, angular to subrounded gravels have also been found in the light-gray layer with a thickness of 8–10 cm and a diameter of 4–6 mm, which were deposited during storm turbulence (Jin et al., 2021). Then,

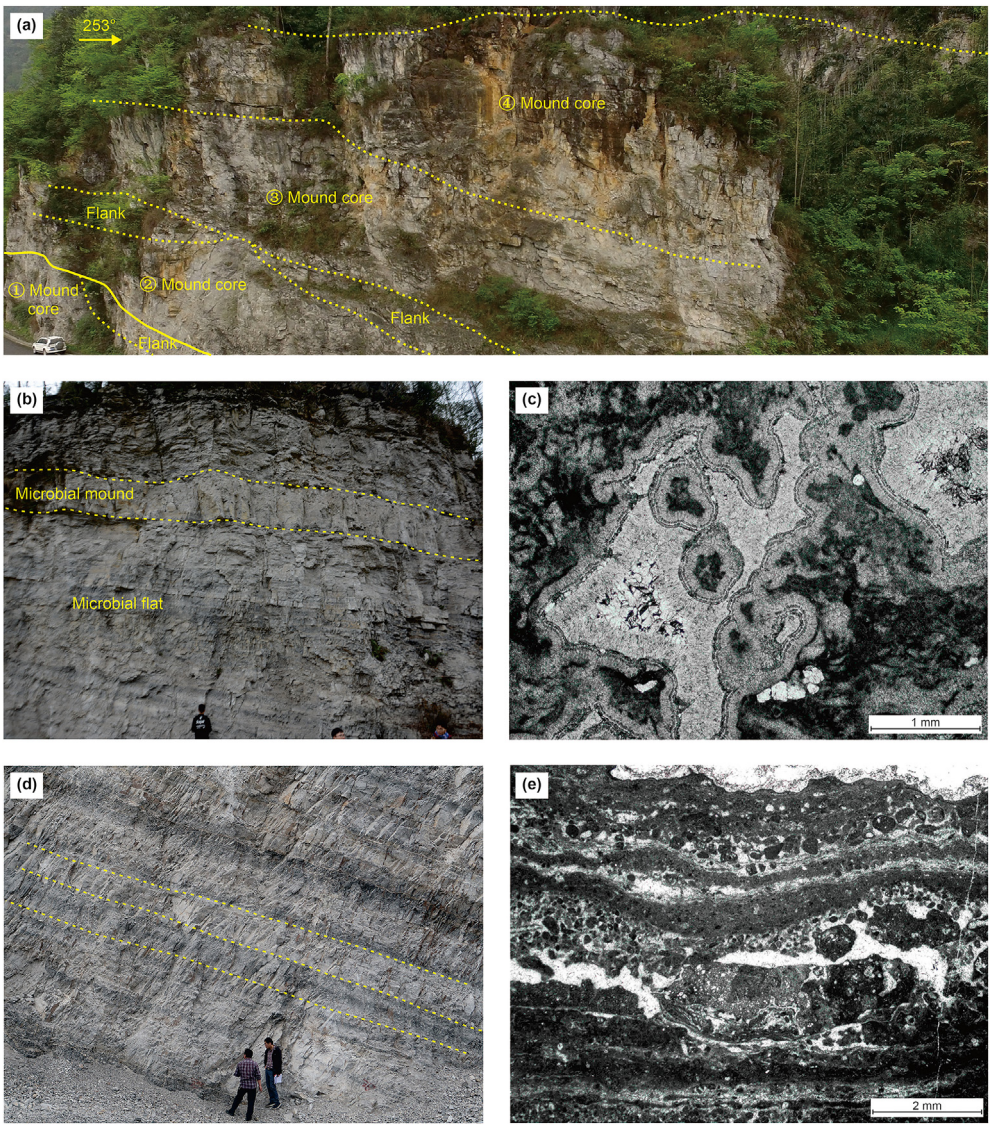

Fig. 8. Macro, meso, and microscopic structures of the Member Deng-2 TEMMCs in the outcrop section Xianfeng, southwestern Sichuan Basin
(a) Four stages of mound structures of TEMMCs in macroscope under unmanned aerial vehicle photography from layer 28 to 31, in outcrop section Village Xianfeng, inside which the mound core and flank could be subdivided; **(b)** mesoscopic characteristics of microbial flat and microbial mound in layer 27, in thickness of (4–5) m and (2–3)m respectively; **(c)** microscopic characteristics of mound core, with clot fabrics bounding together to form fibrous dolomite cemented framework, XF30-2, plane polarized light; **(d)** thin bedded light gray and dark gray couplets develop in layer 44, and dolorudite with graded bedding depositing in the light gray layer; **(e)** light and dark lamination alternated, and the light laminations are composed of microbial binding grains with graded bedding in radial arrangement, XF41-2, plane polarized light. The legends of **a** and **d** are the same as in Fig. 5.

microbial-related fenestral laminations occur at the top of the thin-bedded lagoon deposits, which indicates the beginning of another microbial mound construction cycle.

5. Discussion

5.1. Depositional model of the marginal microbial mound-bank complex of the Member Deng-2

The study region is located on the upper Yangtze craton edge and was primarily deposited during the Deng-2 age in the late Ediacaran period in the southwestern Sichuan Basin, where microbial mound constructions are common along the slightly rimmed platform margin (Zou et al., 2014; Zhou et al., 2015; Zhang, 2017; Song et al., 2018). TJMMCs and TEMMCs have been found out in the marginal microbial mound-bank complexes. The TJMMCs near the fore mound slope horizontally encompasses a thrombolitic mound, stromatolitic mound, and mud mound, which comprise a large-sized mound and small-sized bank in the neighborhood in the macroscope, and are migrated northeastwardly. However, the TEMMCs primarily comprise thick-bedded to massive thrombolitic mounds in the macroscope, which overlie the microbial flat and gradually migrate toward the southwest, showing a thicker microbial flat and small-sized mound with better horizontal connection.

The slightly rimmed platform margin can be subdivided into the windward and leeward sides based on the wind directions (Zhang et al., 2021; Purkis et al., 2019). The windward margin is adjacent to the seaward-facing fore mound slope, which is composed of a microbial mound framework and fore mound in subfacies. However, the leeward margin is bounded by the onshore back mound lagoon horizontally, which comprises subfacies of the microbial mound framework and back mound. Based on the differences in depositional locations, current direction, microbial mound scale,

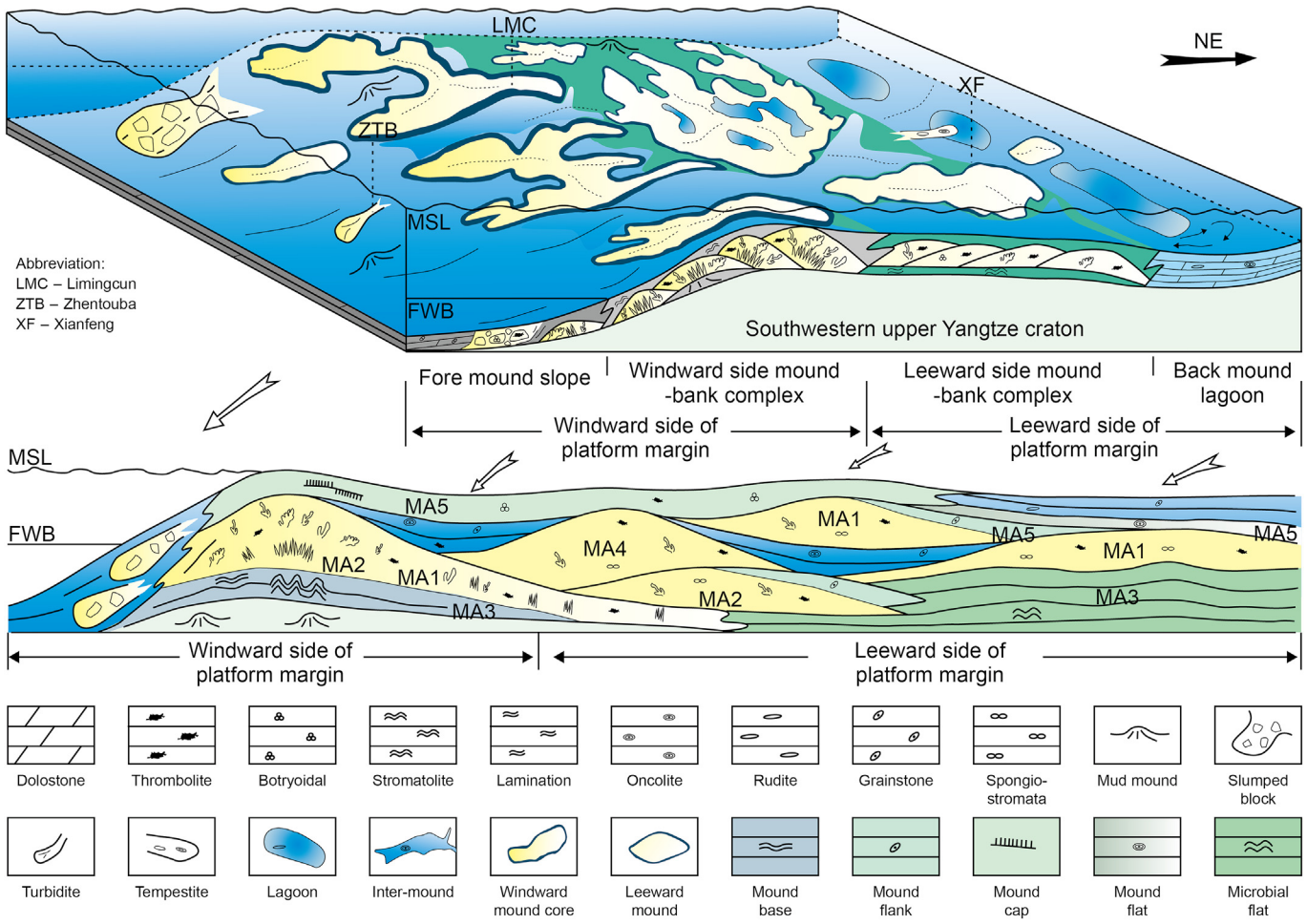

Fig. 9. Depositional model of the Member Deng-2 microbial mound-bank complex in the Dengying Formation, southwestern Sichuan Basin.

and adjacent depositional subfacies, TJMMCs are thought to develop on the southwestern windward margin, while TEMMCs occur along the northeastern leeward margin. The microbial mounds and inter-mound channels are adjacent to each other horizontally and overlie the mud mounds vertically in the TJMMCs. Moreover, the mound base, mound core, mound flank, and mound cap have been identified in microfacies among the TJMMCs. Moreover, different microfacies indicate certain LT, MA and different energy level of sedimentary environments (Table 1). The mound base microfacies primarily comprises stromatolites (LT3) or fenestral stromatolites (LT4), which are related to the MA3 flourishing in the moderate-energy environment of the platform margin or intraplatform flat (Yin et al., 1980; Song et al., 2018). The thrombolites (LT1), spongiostromata stones (LT5), or dendrolites (LT2), related to MA1, MA4, and MA2, respectively, constitute the mound core microfacies growing in the moderate-to high-energy environment of the platform margin or intraplatform flat. Moreover, the oncolite (LT6), aggregated grainstone (LT7), or breccia boundstone lead to the mound flank microfacies. Furthermore, the mound cap microfacies is dominated by fenestral stromatolites (LT4) or botryoidal grapestone (LT8). Both the mound flank and mound cap microfacies are relevant to the coated community of MA5 under a moderate-to high-energy environment of the platform margin or interior platform (Yin et al., 1980; Song et al., 2018). The caption for the abbreviation MA is the same with the Fig. 2.

The TJMMC buildups comprise a large-sized mound and small-sized bank in nearby regions, which continue to grow with transgression and regression backgrounds. However, the mound core, mound flank, and mound flat within the microfacies have been identified. The microbial flat with wavy laminations and a total thickness of 4–5 m comprises the laminated dolomudstones or oncolites (LT6). The thrombolites (LT1) are prominent in the mound core microfacies, while the fenestral stromatolites (LT4) dominate in the mound flank microfacies. The TEMMCs connect each other laterally, showing an overlapping architecture of 'thicker microbial flats in the lower part and small-sized regression microbial mounds in the upper part'. The platform margin of the Member Deng-2 is wide and gentle and the range from the leeward margin to the fore mound slope can reach up to 35 km, as shown in the Fig. 9. The Member Deng-2 marginal microbial mound-bank complexes can be comparable to those in the Exumas Cays portion of Great Bahama Bank, with windward stromatolite mound and leeward oolitic bank (Dravis, 1983; Dill et al., 1986; Andres and Reid, 2006), which grow in neritic, high-energy environments driven by tide and wave.

The platform margin microbial mound depositional model can be correlated with the lateral comparison profile from the outcrop Zhentouba to the borehole W117 as shown in Fig. 10. The microbial mound-bank complexes of the outcrop Zhentouba (TJMMCs) take on an architecture of the microfacies mound core, mound base, mound core, inter-mound, mound core, slumping mound blocks and mound core vertically, which indicate the mound framework subfacies is adjacent to the fore mound subfacies horizontally. As into the outcrop section Xianfang and borehole LL1, the microbial

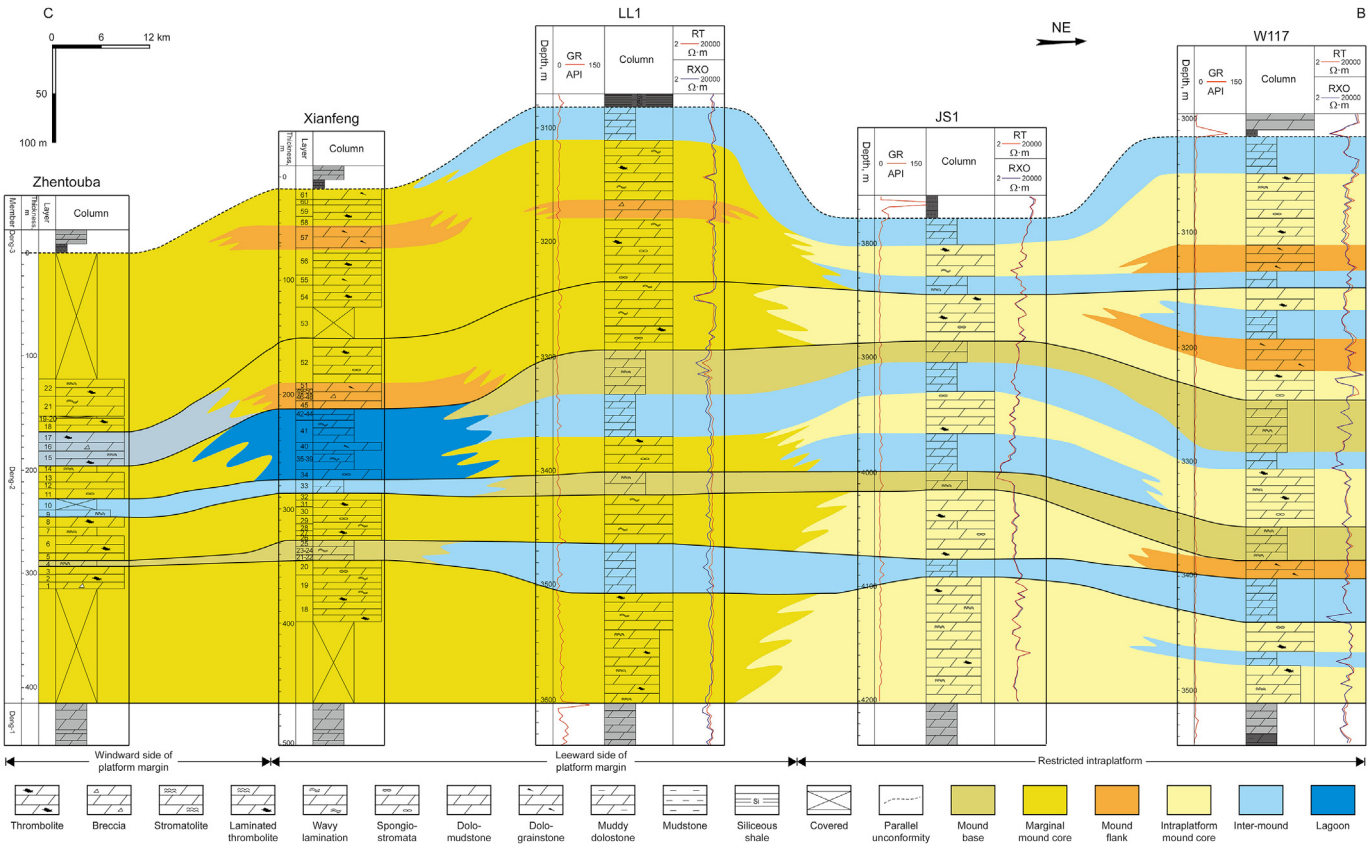

Fig. 10. Lateral correlation profile of the Member Deng-2 mound-bank complex in Dengying Formation from outcrop section Zhentouba to the borehole W117, southwestern Sichuan Basin. The location of the profile can be found in Fig. 1 as marked by C-B.

mound-bank complexes (TEMMCs) are dominated by the microfacies mound core, mound base, mound core, inter-mound, lagoon, mound flank, mound core and mound flank, mound core to inter-mound in order, showing the affinity between the back mound subfacies and the mound framework subfacies. However, the intraplatform microbial mound-bank complexes of the borehole JS1 and W117, are dominated by the microfacies mound core, mound base, mound flank and inter-mound, with larger proportion of mound base and inter-mound microfacies, indicating the coexistence of the microbial flat subfacies and the mound framework subfacies.

5.2. Implications for microbial mound construction and hydrocarbon exploration

The depositional microfacies and structures of microbial mound-bank complexes on the windward margin are different from those on the leeward side as well as the interior platform. The variations between the leeward side and the intraplatform are shown in the 2D seismic section through the boreholes of LL1 and W117, respectively. The microbial mound-bank complex of the Member Deng-2 is 521 m thick in the borehole LL1 and 496 m thick in the borehole W117, which indicates that the microbial mounds on the leeward margin, as shown in the borehole LL1, are much thicker than the intraplatform represented by the borehole W117 (Fig. 11(a)). Moreover, seismic reflection structures lead to different mound microfacies, which are similar to the depositional model shown in Figs. 9 and 10. The mound base microfacies is continuously bedded for reflection both on the time section and instantaneous phase section (Fig. 11(a) and (b)). In addition, the mound core is primarily chaotic or irregularly reflective (Fig. 11(a)) and slightly domal in the instantaneous phase section (Fig. 11(b)), measuring 10–20 km in length and 50–60 m in thickness (Fig. 11(c)). However, the wedge-shaped or lens-like seismic reflections refer to the mound flank (Fig. 11(b) and (c)). The mound cap microfacies lying on the mound core is dominated by intermittent bedded reflection on the instantaneous phase section (Fig. 11(b)), which is much smaller in thickness on the leeward margin (Fig. 11(c)). With regard to the inter-mound channels, they are inferred by the shortly continuous bedded reflection terminated by the domal reflection on both sides (Fig. 11(b)), with a thickness of 100–120 m (Fig. 11(c)). In addition, the mound flat is characterized by the continuous bedded reflection at the top with 60–70 km in length and 15–20 m in thickness (Fig. 11(b) and (c)).

The microbial mound-bank complex constructions on the windward side comprise a large-sized mound and small-sized bank, with high-quality reservoirs overlying each other vertically. However, the leeward margin is dominated by the thicker microbial flat and small-sized mound, with high-quality reservoir connecting laterally. Furthermore, the reservoir evaluation and exploration strategy should be treated in different ways. The overlying mound-bank complex with larger-scale buildups and massive reservoirs should be targeted on the windward side, while the laterally connected mound-bank complex is more common in the leeward platform margin.

Statistically, the hydrocarbon exploration breakthroughs have been made in the microbial mound-bank complex reservoirs all over the world such as in the Sichuan Basin(Liu et al., 2008; Song et al., 2013; Zou et al., 2014; Zhao et al., 2020), Gulf of Mexico (Mancini et al., 2004; Snedden et al., 2020), offshore Brazil (Araujo

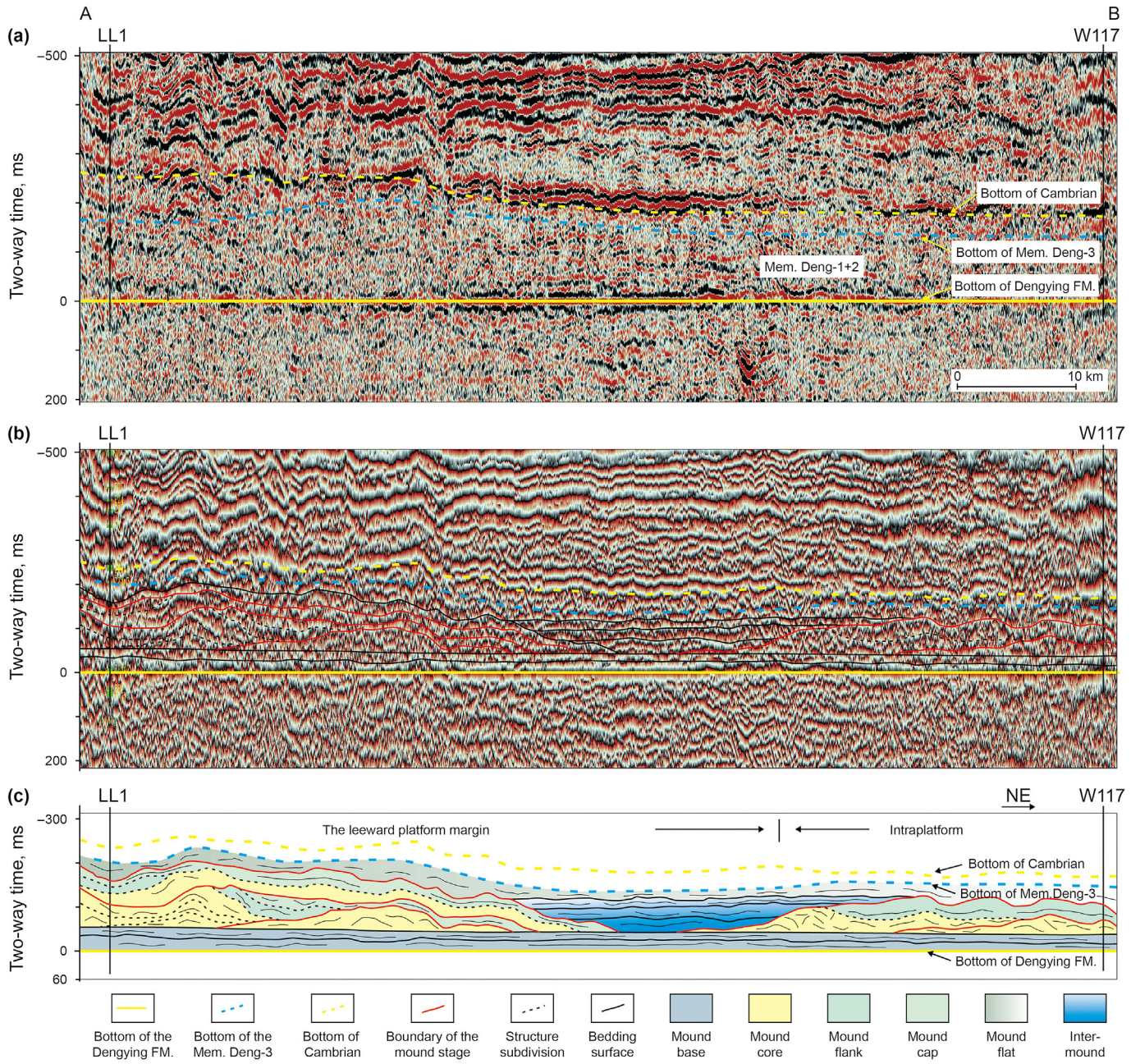

Fig. 11. Seismic reflection characteristics of the leeward margin to the intraplatform microbial mound-bank complex of the Member Deng-2, southwestern Sichuan Basin, with the bottom of the Dengying Formation horizon flattening through the boreholes LL1 and W117.
(a) Microbial mound thickness variations in the 2D seismic time section, of which the leeward margin borehole LL1, with chaotic reflections, is much thicker than intraplatform borehole W117; **(b)** seismic reflection structures of the mound microfacies on the instantaneous phase section, with continuously bedded reflection leading to a mound base and chaotic or marginally domal reflection related to the mound core. The wedge-shaped or lens-like reflections also point to the mound flank, while the intermittent bedded reflections indicate the mound cap. The shortly continuous bedded reflections are correlated to inter-mound channels, and the mound flat is characterized by continuous bedded reflection; **(c)** sketch diagram of **b**, showing the seismic reflection structures. The location of the seismic line can be found in Fig.1 as marked by A-B.

et al., 2022; He et al., 2022), the South Oman Salt Basin (Smodej et al., 2019), eastern Siberia (Tull, 1997; Pelechaty et al., 1996) and Kazakhstan (Collins et al., 2012), whose characteristics are summarized in the Table 2. Recently, the great hydrocarbon exploration breakthrough of Member Deng-2 has been achieved in borehole PT1 on the eastern edge of the Mianyang-Changning intracratonic sag in the Sichuan Basin, SW China (Zhao et al., 2020; Xie et al., 2022). Therefore, the new understanding on reservoir evaluation and exploration strategies of the windward and leeward marginal microbial mound-bank complexes would certainly provide helpful references for future worldwide hydrocarbon exploration processes, particularly in the northeastern edge area of the Mianyang-Changning intracratonic sag in the Sichuan Basin.

6. Conclusions

The microbial mound-bank complex of the Member Deng-2 is well-developed in southwestern Sichuan Basin, with thrombolite (LT1), dendrolite (LT2), stromatolites (LT3), fenestral stromatolites (LT4), spongiostromata stone (LT5), oncolite (LT6), aggregated

Table 2
The composite characteristics of the global oil/gas fields within microbial mound-bank complex reservoirs.

Basin	Geologic time	Formation	Sedimentary facies	Reservoir lithology	Representative oil fields	Oil and gas probable reserves/ production	Sources
Sichuan Basin	Late Ediacaran	Dengying Formation	Intraplatform/Marginal microbial mound-bank complex	Thrombolite, stromatolite, oncolite	Ziyang gasfield	Reserve: 10.2 billion m^3	Liu et al. (2008); Song et al. (2013)
				Thrombolite, stromatolite, oncolite	Weiyuan gasfield	Reserve: 40 billion m^3	Liu et al. (2008); Song et al. (2013)
				Thrombolite, stromatolite, oncolite	Gaoshiti-moxi gasfield	Reserve: 1000 billion m^3	Liu et al. (2008); Zou et al. (2014); Song et al. (2013)
			Marginal microbial mound-bank complex	Thrombolite, stromatolite, oncolite	Penglai gasfield	The Pengtan 1 with a daily production of 1.2198×10^6 m^3	Zhao et al. (2020); Xie et al. (2022)
Pre-Caspian Basin	Late Carboniferous	Visean - Serpukhovian Stage	Isolated carbonate platform margin/slopes	Microbial boundstone	Tengiz field	Reserve: 3×10^9t	Collins et al. (2012)
South-Oman salt basin	Late Ediacaran	Ara Group	Isolated carbonate platform peritidal area	Thrombolite, stromatolite	–	Reserve: 3.5×10^8t	Smodej et al. (2019)
Northern Gulf of Mexico	Late Jurassic	Smackover Formation	Subtidal zone	Thrombolite, stromatolite, oolite	Little Ce- dar Creek field	Reserve: 57.143×10^6t	Mancini et al. (2004);
			Subtidal zone	Thrombolite, stromatolite	Brooklyn Field	Oil production: 0.2143×10^6 t; Gas production: 40×10^6 m^3	Mancini et al. (2004);
Eastern Gulf of Mexico			Ramp grain bank/subtidal zone	Thrombolite, stromatolite, grainstone	Appleton field	Production : 0.384×10^6 t	Mancini et al. (2004)
			Ramp grain bank	Thrombolite, stromatolite	Vocation field	Production : 0.323×10^6 t	Mancini et al. (2004)
Santos basin/ Campos basin	Early Cretaceous	–	Lacustrine carbonate platform-slope facies	Thrombolite, stromatolite, oolite	Pre-Salt field	Oil reserve: 1.14×10^9 t	Araujo et al. (2022); He et al. (2022)
East Siberia Basin	Mesoproterozoic to Late Cambrian	–	Ramp tidal microbial mat and microbial bank	Stromatolite	East Siberia field	Gas reserve: 1.13268×10^{12} m^3; Oil reserve: 0.86×10^9 t	Tull (1997); Pelechaty et al. (1996)

grainstone (LT7) and botryoidal grapestone (LT8) in lithologic textures, which are associated with the microbe community of *Gloeorrh alveus* Tsao et Zhao and *Trachysphaeridium* sp. (MA1), *Balios*, *Renaclis*, *Paleomicrocystis*, *Actinophycus divaricatus* Yin (sp. Nov.), *Phacelofimbria emeishanensis* Tsao et Zhao and *Epiphiton-resembling* (MA2), *Acus Muricatus* Tsao et Zhao, *Praesolenopora fascicularis* Cao et Zhao and *Siphonia* sp. (MA3), *Tortofimria dictyotos* Tsao et Zhao (MA4) and coated microbes (MA5). Based on the composite analysis of 'depositional fabrics-lithology-microfacies', a subfacies association between a fore mound, mound framework, and back mound has been proposed based on water depth, current direction, energy level and lithologic assemblages. The microfacies of the mound base, mound core, mound flank, mound cap and mound flat could be recognized among the mound framework subfacies. The mound base microfacies is built by the MA3 and mostly composed of LT3 or LT4. However, the mound core microfacies is dominated by LT1, LT5 or LT2, resulting from MA1, MA4 and MA2 respectively. The LT6, LT7 or breccia boundstone consist of the mound flank microfacies while the LT4 or LT8 occupy the mound cap microfacies. The laminated dolomudstone or oncolite (LT6) occur in the mound flat microfacies. The mound flank, mound cap and mound flat microfacies are all relevant to the MA5.

Two construction types of marginal microbial mound-bank complex have been determined based on deposition location, mound scale, migration direction, and sedimentary facies association. TJMMCs develop along the windward margin owing to their proximity to the seaward fore mound subfacies, with six stages of northeastwardly migrated microbial mound on top of the mud mound, exhibiting the characteristics of large-sized mounds and small-sized banks in the surrounding area. TEMMCs primarily occur on the leeward margin, resulting from the presence of onshore back mound subfacies, with the four stages of smaller southwestward migrated microbial mounds existing on a thicker microbial flat.

The platform margin microbial mound depositional model of the southwestern Sichuan Basin would provide references for the understanding of the Ediacaran microbial mound construction process as well as the strategy of future worldwide hydrocarbon explorations, which could be correlated to the different seismic reflection structures. The vertically overlying massive high-quality microbial mound-bank complex reservoirs are typically targeted on the windward margin with larger-sized mound and smaller-sized bank. However, the laterally-connected mound-bank complex reservoirs would be emphasized on the leeward margin with thicker microbial flat and smaller-sized mound.

Declaration of competing interest

The authors declare that they have no known competing financial interests or personal relationships that could have appeared to influence the work reported in this paper.

Acknowledgements

This study was jointly funded by projects supported by the National Natural Science Foundation of China (Grant No. 41872150), the Joint Funds of the National Natural Science Foundation of China (Grant No. U19B6003) and Major Scientific and Technological Projects of CNPC during the 13th five-year plan (No. 2019A-02–10).

The authors would also like to thank the editors and anonymous reviewers for their constructive suggestions for the manuscript improvement.

References

Andres, M.S., Reid, R.P., 2006. Growth morphologies of modern marine stromatolites: a case study from Highborne Cay, Bahamas. Sediment. Geol. 185, 319–328. https://doi.org/10.1016/j.sedgeo.2005.12.020.

Araujo, C.C., Madrucci, V., Homewood, P., Mettraux, M., Ramnani, C.W., Spadini, A.R., 2022. Stratigraphic and sedimentary constraints on presalt carbonate reservoirs of the South Atlantic Margin, Santos Basin, offshore Brazil. AAPG (Am. Assoc. Pet. Geol.) Bull. 106, 2513–2546. https://doi.org/10.1306/08082219218.

Chen, Z., Bengtson, S., Zhou, C.M., Hua, H., Yue, Z., 2008. Tube structure and original composition of Sinotubulites: shelly fossils from the late Neoproterozoic in southern Shaanxi, China. Lethaia 41, 37–45. https://doi.org/10.1111/j.1502-3931.2007.00040.x.

Chen, Z., Zhou, C.M., Xiao, S.H., Wang, W., Guan, C.G., Hua, H., Yuan, X.L., 2014. New Ediacara fossils preserved in marine limestone and their ecological implications. Sci. Rep. 4, 4180. https://doi.org/10.1038/srep04180.

Chen, Y.N., Shen, A.J., Pan, L.Y., Zhang, J., Wang, X.F., 2017. Features, origin and distribution of microbial dolomite reservoirs: a case study of 4th Member of Sinian Dengying Formation in Sichuan Basin, SW China. Petrol. Explor. Dev. 44, 745–757. https://doi.org/10.1016/S1876-3804(17)30085-X.

Collins, J., Kenter, J., Playton, T., 2012. Characterization and controls on slope geometry, framework and internal heterogeneity in the unit 1 Tengiz Field (Kazakhstan), and comparison with outcrop analogs. Abstract. In: Proceedings of American Association of Petroleum Geologists Annual Meeting, pp. 79–88. CA.

Deng, S.H., Fan, R., Li, X., Zhang, S., Zhang, B.M., Lu, Y.Z., 2015. Subdivision and correlation of the Sinian (Ediacaran) system in the Sichuan Basin and its adjacent area. J. Stratigr. 39, 239–254. https://doi.org/10.19839/j.cnki.dcxzz.2015.03.001 (in Chinese).

Dickson, J.A.D., 1965. A modified staining technique for carbonates in thin section. Nature 205, 587. https://doi.org/10.1038/205587a0.

Dill, R.F., Shinn, E.A., Jones, A.T., Kelly, K., Steinen, R.P., 1986. Giant subtidal stromatolites forming in normal salinity waters. Nature 324, 55–58. https://doi.org/10.1038/324055a0.

Ding, Y., Chen, D.Z., Zhou, X.Q., Guo, C., Huang, T.Y., Zhang, G.J., 2019. Cavity-filling dolomite speleothems and submarine cements in the Ediacaran Dengying microbialites, South China: responses to high-frequency sea-level fluctuations in an 'aragonite-dolomite sea'. Sedimentology 66, 2511–2537. https://doi.org/10.1111/sed.12605.

Ding, Y., Li, Z.W., Liu, S.G., Song, J.M., Zhou, X.Q., Sun, W., Zhang, X.H., Li, S.J., Ran, B., Peng, H.L., Li, Z.Q., Wang, H., Chen, D.Z., 2021. Sequence Stratigraphy and Tectono-Depositional Evolution of a Late Ediacaran Epeiric Platform in the Upper Yangtze Area, South China. Precambrian Research 354, 106077. https://doi.org/10.1016/j.precamres.2020.106077.

Dravis, J.J., 1983. Hardened subtidal stromatolites, Bahamas. Science 219, 385–386. https://doi.org/10.1126/science.219.4583.385.

Du, J.H., Zou, C.N., Xu, C.C., He, H.Q., Shen, P., Yang, Y.M., Li, Y.L., Wei, G.Q., Wang, Z.C., Yang, Y., 2014. Theoretical and technical innovations in strategic discovery of a giant gas field in Cambrian Longwangmiao Formation of central Sichuan paleo-uplift, Sichuan Basin. Petrol. Explor. Dev. 41, 294–305. https://doi.org/10.1016/S1876-3804(14)60035-5.

Feng, Z.Z., 2019. A review on the definitions of terms of sedimentary facies. J. Palaeogeogr. 8, 321–331. https://doi.org/10.1186/s42501-019-0045-3.

Flügel, E., 2010. Microfacies of Carbonate Rocks: Analysis, Interpretation and Application. Springer-Verlag, Berlin, pp. 680–711. https://doi.org/10.1007/978-3-642-03796-2.

He, S., Li, G.R., Wu, C.R., Liu, S.G., Zhang, Z.M., Su, Y.S., Zhu, Y.X., He, Z., Ren, J., Wang, Y.C., Zhou, W., Wang, Y.J., 2022. Sedimentary filling characteristics and controlling factors of lacustrine microbial carbonates sequence in the Santos Basin, Brazil. Petrol. Explor. Dev. 49, 785–796. https://doi.org/10.1016/s1876-3804(22)60310-0.

Hu, M.Y., Gao, D., Wei, G.Q., Yang, W., Xie, W.R., 2019. Sequence stratigraphy and facies architecture of a mound-shoal-dominated dolomite reservoir in the late Ediacaran Dengying Formation, central Sichuan Basin, SW China. Geol. J. 54, 1653–1671. https://doi.org/10.1002/gj.3261.

Hua, H., Chen, Z., Yuan, X.L., 2007. The advent of mineralized skeletons in Neoproterozoic Metazoa—new fossil evidence from the Gaojiashan Fauna. Geol. J. 42, 263–279. https://doi.org/10.1002/gj.1077.

Jiang, H., Zhang, B.M., Xu, C.C., et al., 2016. Discovery of Intra-cratonic Rift in the Upper Yangtze and its Coutrol Effect on the Formation of Anyue Giant Gas Field. Acta Petrolei Sinica 37, 1–16. https://doi.org/10.7623/syxb201601001 (in Chinese).

Jin, X., Song, J.M., Liu, S.G., Li, Z.W., Wen, L., Sun, W., Luo, B., Zhang, X.H., Zhou, G., Peng, H.L., 2021. Characteristics and geological implications of Dengying Formation tempestites in the periphery of the Sichuan Basin. Nat. Gas. Ind. 41, 39–49. https://doi.org/10.3787/j.issn.1000-0976.2021.10.005 (in Chinese).

Knoll, A.H., 2015. Paleobiological perspectives on early microbial evolution. Cold Spring Harbor Perspect. Biol. 7. https://doi.org/10.1101/cshperspect.a018093.

Lan, C.J., Xu, Z.H., Ma, X.L., Hu, C., Chen, H.R., Zou, H.Y., 2019. Development and distribution of mound-shoal complex in the Sinian Dengying Formation, Sichuan Basin and its control on reservoirs. Acta Pet. Sin. 40, 1069–1084. https://doi.org/10.17623/syxb201909005 (in Chinese).

Li, S.J., Gao, P., Huang, B.Y., Wang, H.J., Wo, Y.J., 2018. Sedimentary constraints on the tectonic evolution of Mianyang-Changning trough in the Sichuan Basin. Oil Gas Geol. 39, 889–898. https://doi.org/10.11743/ogg20180504 (in Chinese).

Liu, S.G., Ma, Y.S., Sun, W., Cai, X.Y., Liu, S., Huang, W.M., Xu, G.S., Yong, Z.Q., Wang, G.Z., Wang, H., Pan, C.L., 2008. Studying on the differences of Sinian natural gas pools between Weiyuan gas field and Ziyang gas-brone area, Sichuan Basin. Acta Geol. Sin. 82, 328–337. https://doi.org/10.1007/s11442-008-0201-7 (in Chinese).

Liu, J.J., Li, W., Zhang, B.M., Zhou, H., Yuan, X.H., Shan, X.Q., Zhang, J., Deng, S.H., Gu, Z.D., Fan, R., Wang, Y.J., Li, X., 2015. Sedimentary paleogeography of Sinian in upper Yangtze region. J. Palaeogeogr. 17, 735–753. https://doi.org/10.7605/gdlxb.2015.06.061 (in Chinese).

Liu, S.G., Song, J.M., Luo, P., Qing, H.R., Lin, T., Sun, W., Li, Z.W., Wang, H., Peng, H.L., Yu, Y.Q., Long, Y., Wan, Y.B., 2016. Characteristics of Microbial Carbonate Reservoir and its Hydrocarbon Exploring Outlook in the Sichuan Basin, China. Journal of Chengdu University of Technology (Science & Technology Edition) 43, 129–152. https://doi.org/10.3969/j.issn.1671-9727.2016.02.01 (in Chinese).

Liu, S.G., Deng, B., Jansa, L., Zhong, Y., Sun, W., Song, J.M., Wang, G.Z., Wu, J., Li, Z.W., Tian, Y.H., 2017. The early cambrian Mianyang-changning intracratonic sag and its control on Petroleum accumulation in the Sichuan Basin, China. Geofluids 8, 1–17. https://doi.org/10.1155/2017/6740892.

Liu, S.G., Sun, W., Luo, Z.L., Song, J.M., Zhong, Y., Tian, Y.H., Peng, H.L., 2013. Xingkai Taphrogenesis and Petroleum Exploration from Upper Sinian to Cambrian Strata in Sichuan Basin, China. Journal of Chengdu University of Technology (Science & Technology Edition 40, 511–520. https://doi.org/10.3969/j.issn.1671-9727.2013.05.03 (in Chinese).

Longman, M.W., 1981. A Process Approach to Recognizing Facies of Reef Complexes. SEPM special publication 30, 9–40. https://doi.org/10.2110/pec.81.30.0009.

Luo, P., Wang, S., Li, P.W., Song, J.M., Jin, T.F., Wang, G.Q., Yang, S.S., 2013. Review and prospectives of microbial carbonate reservoirs. Acta Sedimentol. Sin. 31, 807–823. https://doi.org/10.14027/j.cnki.cjxb.2013.05.005 (in Chinese).

Luo, B., Yang, Y.M., Luo, W.J., Wen, L., Wang, W.Z., Chen, K., 2015. Controlling factors and distribution of reservoir development in Dengying Formation of paleouplift in central Sichuan Basin. Acta Pet. Sin. 36, 416–426. https://doi.org/10.7623/syxb201504003 (In Chinese).

Luo, Y., Tan, X., et al., 2022. Sedimentary characteristics of the Ediacaran microbial carbonates and their geological implications:a case study of the Member 4 of Dengying Formation from Wellblock MX8 in central Sichuan Basin. J. Palaeogeogr. 24, 278–291. https://doi.org/10.7605/gdlxb.2022.02.017 (in Chinese).

Mancini, E.A., Llinas, J.C., Parcell, W.C., Aurell, M., Badenas, B., Leinfelder, R.R., Benson, D.J., 2004. Upper Jurassic thrombolite reservoir play, northeastern Gulf of Mexico. AAPG (Am. Assoc. Pet. Geol.) Bull. 88, 1573–1602. https://doi.org/10.1306/06210404017.

Pelechaty, S.M., Kaufman, A.J., Grotzinger, J.P., 1996. Evaluation of $\delta^{13}C$ chemostratigraphy for intrabasinal correlation: Vendian strata of northeast Siberia. GSA Bulletin 108, 992–1003. https://doi.org/10.1130/0016-7606(1996)108<0992:EOCCFI>2.3.CO;2.

Peng, H.L., Liu, S.G., Song, J.M., Sun, W., Yin, K.W., 2014. Characteristics of microbial carbonate rocks in upper sinian Dengying Formation of Micang Mountains, North sichuan, China. J. Chengdu Univ. Technol. (Sci. Technol. Ed.) 41, 181–191. https://doi.org/10.3969/j.issn.1671-9727.2014.02.08 (in Chinese).

Purkis, S.J., Harris, P.M., Cavalcante, G., 2019. Controls of depositional facies patterns on a modern carbonate platform: insight from hydrodynamic modeling. Deposit. Rec. 5, 421–437. https://doi.org/10.1002/dep2.61.

Qian, Y.X., Feng, J.F., He, Z.L., Zhang, K.Y., Jin, T., Dong, S.F., You, D.H., Zhang, Y.D., 2017. Applications of petrography and isotope analysis of micro-drill samples to the study of genesis of grape-like dolomite of the Dengying Formation in the Sichuan Basin. Oil Gas Geol. 38, 665–676. https://doi.org/10.11743/ogg20170404 (in Chinese).

Smodej, J., Reuning, L., Becker, S., Kukla, P.A., 2019. Micro- and nano-pores in intrasalt, microbialite-dominated carbonate reservoirs, Ara Group, South-Oman salt basin. Mar. Petrol. Geol. 104, 389–403. https://doi.org/10.1016/j.marpetgeo.2019.03.036.

Snedden, J.W., Cunningham, R.C., Virdell, J.W., 2020. The northern Gulf of Mexico offshore super basin: reservoirs, source rocks, seals, traps, and successes. AAPG (Am. Assoc. Pet. Geol.) Bull. 104, 2603–2642. https://doi.org/10.1306/09092020054.

Song, J.M., Liu, S.G., Sun, W., Wu, W.H., Wang, G.Z., Peng, H.L., Tian, Y.H., Zhong, Y., 2013. Control of Xingkai taphrogenesis on Dengying Formation high quality reservoirs in upper Sinian of Sichuan Basin, China. J. Chengdu Univ. Technol. (Sci. Technol. Ed.) 40, 658–670. https://doi.org/10.3969/j.issn.1671-9727.2013.06.05 (In Chinese).

Song, J.M., Liu, S.G., Li, Z.W., Luo, P., Yang, D., Sun, W., Peng, H.L., Yu, Y.Q., 2017. Characteristics and controlling factors of microbial carbonate reservoirs in the upper sinian Dengying Formation in the Sichuan Basin, China. Oil Gas Geol. 38, 741–752. https://doi.org/10.11743/ogg20170411 (in Chinese).

Song, J.M., Liu, S.G., Qing, H.R., Jansa, L., Li, Z.W., Luo, P., Yang, D., Sun, W., Peng, H.L., Lin, T., 2018. The depositional evolution, reservoir characteristics, and controlling factors of microbial carbonates of Dengying Formation in upper Neoprotozoic, Sichuan Basin, Southwest China. Energy Explor. Exploit. 36, 591–619. https://doi.org/10.1177/0144598717743995.

Sun, W., Liu, S.G., Song, J.M., Deng, B., Wang, G.Z., Wu, J., Jiao, K., Li, J.X., Ye, Y.H., Li, Z.W., Li, Z.Q., 2017. The Formation Process and Characteristics of Ancient and Deep Carbonate Petroleum Reservoirs in Superimposed Basins: A Case Study of Sinian (Ediacaran) Dengying Formation in the Sichuan Superimposed Basin, China. Journal of Chengdu University of Technology (Science & Technology Edition) 44, 257–285. https://doi.org/10.3969/j.issn.1671-9727.2017.03.01 (in Chinese).

Tomas, S., Homann, M., Mutti, M., Amour, F., Christ, N., Immenhauser, A., Agar, S.M., Kabiri, L., 2013. Alternation of microbial mounds and ooid shoals (Middle Jurasssic, Morocco): response to paleoenvironmental changes. Sediment. Geol. 294, 68–82. https://doi.org/10.1016/j.sedgeo.2013.05.008.

Tomitani, A., Knoll, A.H., Cavanaugh, C.M., Ohno, T., 2006. The evolutionary diversification of cyanobacteria: Molecular phylogenetic and paleontological perspectives. Proc. Natl. Acad. Sci. USA 103, 5442–5447. https://doi.org/10.1073/pnas.0600999103.

Tucker, M.E., 1985. Shallow-Marine Carbonate Facies and Facies Models. Geological Society London Special Publications 18, 147–169. https://doi.org/10.1144/gsl.sp.1985.018.01.08.

Tull, S.J., 1997. The diversity of hydrocarbon habitat in Russiaa. Petrol. Geosci. 3, 315–325. https://doi.org/10.1144/petgeo.3.4.315.

Wang, Y., Wang, S.Y., Yan, H.J., Zhang, Y.J., Li, J.Z., Ma, D.B., 2021. Microbial carbonate sequence architecture and depositional environments of member IV of the late Ediacaran Dengying Formation, Gaoshiti-Moxi area, Sichuan Basin, southwest China. Geol. J. 56 (8), 3992–4015. https://doi.org/10.1002/gj.4146.

Wei, G.Q., Chen, G.S., Du, S.M., Zhang, L., Yang, W., 2008. Petroleum systems of the oldest gas field in China: Ediacaran gas pools in the Weiyuan gas field, Sichuan Basin. Mar. Petrol. Geol. 25, 371–386. https://doi.org/10.1016/j.marpetgeo.2008.01.009.

Wei, G.Q., Du, J.H., Xu, C.C., Zou, C.N., Yang, W., Shen, P., Xie, Z.Y., Zhang, J., 2015a. Characteristics and accumulation modes of large gas reservoirs in Sinian-Cambrian of Gaoshiti-Moxi region, Sichuan Basin. Acta Pet. Sin. 36, 1–12. https://doi.org/10.7623/syxb201501001 (in Chinese).

Wei, G.Q., Yang, W., Du, J.H., Xu, C.C., Zou, C.N., Xie, W.R., Zeng, F.Y., Wu, S.J., 2015b. Geological characteristics of the sinian- early cambrian intracratonic rift, Sichuan Basin. Nat. Gas. Ind. 35, 24–35. https://doi.org/10.3787/j.issn.1000-0976.2015.01.003 (in Chinese).

Wen, L., Yang, Y.M., You, C.Q., Zhang, X.H., Peng, H.L., Wang, W.Z., Luo, B., Luo, W.J., 2016. Characteristics of Dengying Fm sedimentary sequence in the central-western Sichuan Basin and their controlling effect on gas accumulation. Nat. Gas. Ind. 36, 8–17. https://doi.org/10.1016/j.ngib.2017.02.004 (in Chinese).

Wilson, J.L., 1975. Carbonate facies in geologic history. Springer, Berlin, pp. 20–55. https://doi.org/10.1007/978-1-4612-6383-8.

Xie, J.R., Zhang, Z.L., Zhong, Y., Yan, W., Li, K.Y., He, Y., Zhao, L.K., Long, H.Y., Zhang, B.S., Qiao, Y.P., 2022. New understanding and potential analysis of natural gas exploration of the Dengying Member 2 in central-northern area of Sichuan Basin. Marine Origin Petrol. Geol. 27, 225–235. https://doi.org/10.3969/j.issn.1672-9854.2022.03.001 (in Chinese).

Xing, F.C., Hou, M.C., Lin, L.B., Xu, S.L., Hu, H.R., 2015. The records and its dynamic genesis discussion of tectonic movement during the Late Sinian and the Early Cambrian of Sichuan Basin. Earth Sci. Front. 22, 115–125. https://doi.org/10.13745/j.esf.2015.01.010 (in Chinese).

Xu, Z.H., Lan, C.J., Ma, X.L., Hu, C., Chen, H.R., Li, P.P., Zou, H.Y., 2020. Sedimentary models and physical properties of mound-shoal complex reservoirs in Sinian Dengying Formation, Sichuan Basin. Earth Sci. 45, 1281–1294. https://doi.org/10.3799/dqkx.2019.138 (in Chinese).

Xu, Z.H., Lan, C.J., Zhang, B.J., Hao, F., Lu, C.J., Tian, X.W., Zou, H.Y., 2022. Impact of diagenesis on the microbial reservoirs of the terminal Ediacaran Dengying Formation from the central to northern Sichuan Basin, SW China. Mar. Petrol. Geol. 146, 105924. https://doi.org/10.1016/j.marpetgeo.2022.105924.

Yang, Y.M., Yang, Y., Yang, G., Song, J.R., Wen, L., Deng, C.G., Xia, M.L., Ran, Q., Duan, G.L., Luo, B., Xie, B., 2019. Gas accumulation conditions and key exploration & development technologies of Sinian and Cambrian gas reservoirs in Anyue gas field. Acta Pet. Sin. 40, 493–508. https://doi.org/10.3866/PKU.WHXB201112303 (in Chinese).

Yang, W., Wei, G.Q., Xie, W.R., Jin, H., Zeng, F.Y., Su, N., Sun, A., Ma, S.Y., Shen, J.H., Wu, S.J., 2020. Hydrocarbon accumulation and exploration prospect of mound-shoal complexes on the platform margin of the fourth member of Sinian Dengying Formation in the east of Mianzhu-Changning intracratonic rift, Sichuan Basin, SW China. Petrol. explor. develop. 47, 1262–1274. https://doi.org/10.1016/S1876-3804(20)60134-9.

Yin, J.C., Ding, L.F., He, T.G., He, T.G., Li, S.L., Shen, L.J., 1980. The Palaeontology and Sedimentary Environment of the Sinian System in Emei to Ganluo Area, Sichuan. Chengdu, Sichuan People Press (in Chinese).

Zhai, X.F., Luo, P., Gu, Z.D., Jiang, H., Zhang, B.M., Wang, Z.C., Wang, T.S., Wu, S.T., 2020. Microbial mineralization of botryoidal laminations in the upper Ediacaran dolostones, western Yangtze platform, SW China. J. Asian Earth Sci. 195, 104333–104344. https://doi.org/10.1016/j.jseaes.2020.104334.

Zhang, B.M., 2017. Geology and Genetic Origin of Marine Carbonate Reservoir in China. Science Press, Beijing, pp. 158–174 (in Chinese).

Zhang, Y.B., Tang, Z.Y., Chen, J.G., 1996. The classification and application of boundstone. Nat. Gas Explorat. Develop. 19, 24–33 (in Chinese).

Zhang, J.L., Hu, M.Y., Feng, Z.H., Li, Q., He, X.X., Zhang, B., Yan, B., Wei, G.Q., Zhu, G.Y., Zhang, Y., 2021. Types of the Cambrian platform margin mound-shoal complexes and their relationship with paleogeomorphology in Gucheng area, Tarim Basin, NW China. Petrol. explor. develop. 48, 110–122. https://doi.org/10.1016/s1876-3804(21)60008-3.

Zhao, G.C., Wang, Y.J., Huang, B.C., Dong, Y.P., Li, S.Z., Zhang, G.W., Yu, S., 2018. Geological reconstructions of the east Asian blocks: from the breakup of rodinia to the assembly of Pangea. Earth Sci. Rev. 186, 262–286. https://doi.org/10.1016/j.earscirev.2018.10.003.

Zhao, L.Z., Wang, Z.C., Yang, Y., Duan, S.F., Wei, G.Q., Luo, B., Wen, L., Ma, S.U., Feng, Q.F., Liu, J.J., Sun, X.P., Xie, W.R., 2020. Important discovery in well Pengtan 1 in the second member of the Dengying Formation in the Sichuan Basin and its significance. China Petrol. Explorat. 25, 1–12. https://doi.org/10.3969/J.ISSN.1672-7703.2020.03.001 (In Chinese).

Zhao, W.Z., Wang, X.F., Wang, X., Wang, K., Shen, A.J., 2022. Stratigraphic sequence re-determination and lithofacies palaeogeographical characteristics of the sinian Dengying Formation in Sichuan Basin. J. Palaeogeogr. 24, 854–872. https://doi.org/10.3866/PKU.WHXB201112303 (in Chinese).

Zhou, H., Li, W., Zhang, B.M., Liu, J.J., Deng, S.H., Zhang, S.B., Shan, X.Q., Zhang, J., Wang, X.B., Jiang, H., 2015. Formation and evolution of upper sinian to lower cambrian intraplat formal Basin in Sichuan Basin. Acta Pet. Sin. 36, 310–323. https://doi.org/10.7623/syxb201503006 (in Chinese).

Zhou, C.M., Yuan, X.L., Xiao, S.H., Chen, Z., Hua, H., 2019. Ediacaran composite strata and age constraints in China. Scientia Sinica Terrae 49, 7–25. https://doi.org/10.1360/N072017-00230 (in Chinese).

Zou, C.N., Du, J.H., Xu, C.C., Wang, Z.C., Zhang, B.M., Wei, G.Q., Wang, T.S., Yao, G.S., Deng, S.H., Liu, J.J., Zhou, H., Xu, A.N., Yang, Z., Jiang, H., Gu, Z.D., 2014. Formation, distribution, resource potential, prediction and discovery of Sinian-Cambrian super-giant gas field, Sichuan Basin, SW China. Petrol. Explor. Dev. 41, 278–293. https://doi.org/10.1016/S1876-3804(14)60036-7 (in Chinese).